King Saud University

Arabian Journal of Chemistry

www.ksu.edu.sa
www.sciencedirect.com

ORIGINAL ARTICLE

Synthesis, spectroscopic characterization and study the effect of gamma irradiation on VO^{2+}, Mn^{2+}, Zn^{2+}, Ru^{3+}, Pd^{2+}, Ag^+ and Hg^{2+} complexes and antibacterial activities

S.A. Aly *, D. Elembaby

Department of Environmental Biotechnology, Genetic Engineering and Biotechnology Research Institute, University of Sadat City, Egypt

Abstract Novel complexes of VO^{2+}, Mn^{2+}, Zn^{2+}, Ru^{3+}, Pd^{2+}, Ag^+ and Hg^{2+} have been prepared by reacting their metal salts with ligand, named (4-(4-chlorophenyl)-1-(2-(phenylamino) acetyl) thiosemicarbazone). Study of synthesized metal complexes was confirmed by different analytical and spectral techniques (^{1}H NMR, MS, FT-IR, UV–Vis, EPR and Powder X-ray diffraction), thermogravimetric studies as well as molecular modeling. FT-IR spectra showed that the compound behave as neutral or monobasic tetradentate. In case of complexes of Mn^{2+}, Zn^{2+}, Ag^+ and VO^{2+}, through (N2—H), (C=O) or (C—O) groups. While, the ligand behave as neutral bidentate in case of complexes with Pd^{2+} and Hg^{2+}. X-ray diffraction pattern of Mn^{2+}, Pd^{2+} and Ag^+ complexes before and after irradiation are recorded. XRD studies exhibited that decrease in the crystalline size of sample Mn^{2+} as compared of samples Ag^+ and Pd^{2+} upon irradiation and irradiation influenced the crystallinity of the complexes. The possible structures of the ligand, Mn^{2+}, Pd^{2+} and Hg^{2+} complexes have been computed by means of the molecular mechanic calculations using the hyper chem. 8.03 molecular modeling program. The bond length, bond angle, HOMO, LUMO and dipole moment have been studied to verify the geometry of Mn^{2+}, Pd^{2+} and Hg^{2+} complexes. The effect of gamma irradiation was investigated by recording the new results of pervious spectroscopic techniques and other measurements. Thermal studies of these chelates before and after γ-irradiation showed that the complexes after γ-irradiation were more thermally stable than before γ-irradiation. The compound and its metal complexes have been experienced

* Corresponding author.
  E-mail address: samar.mostafa@gebri.usc.edu.eg (S.A. Aly).
Peer review under responsibility of King Saud University.

Production and hosting by Elsevier

for their inhibitory outcome on the growth of microorganisms against gram positive and gram negative. The results proved that the complexes **B₁–B₇** have potent antibacterial activity as compared to that of ligand.

1. Introduction

Thiosemicarbazones are artificially active pharmacophores and their activities strengthen chelation with metal ions. The transition metal complexes with these compounds have elevated interest with several researchers and they persist to be subjected to numerous applications. Thiosemicarbazones generally operate as chelating compounds for transition metal ions by bonding via the sulphur and azomethine nitrogen atoms; while, in a few cases they act as monodentate ligand wherever connect via sulphur only (Murali et al., 2009).

Metal ions are necessary for biological purposes like iron which is found in hemoglobin and myoglobin; zinc which is required to superoxide dismutase enzyme; and also, sodium and potassium which play vital roles in homeostatic processes. Silver salts have been used as an antiseptic collyrium to shun ophthalmic infections in newborns (Gustavo et al., 2012).

X-ray diffraction patterns of ferric, copper and zinc of complexes of thiosemcarbazide derivatives have been synthesized. These complexes exhibit different physical properties. Ferric complex has triclinic crystal structure, however copper and zinc complexes of ligand have monoclinic crystal structures with diverse unit cell parameters by using x-ray powder diffraction. These complexes showed significant activities against microorganisms and fungi as compared to that of ciprofloxacin treatment (Gavhane et al., 2015).

Radiation is extensively used in the biomaterials science for surface modification, disinfection and to develop *bulk* possessions. Radiation is also used for improvement of biochips, and in situ photopolymerizable of bioglues. The energy sources most usually used in the irradiation of biomaterials are great-energy electrons, gamma radiation and UV. Surface adjustment includes placement of selective chemical moieties on the surface of a material by chemical reactions to develop bio interaction for cell connection and propagation. The exposure of a polymer to radiation, specially ionizing radiation, can is due to chain scission or crosslinking with variation in bulk and surface properties. Disinfection by irradiation is considered to inactivate greatest pathogens from the surface of biomedical processes. An indication of the use of gamma and UV radiation to develop surface of material compatibility, bulk things and surface things for wear resistance, development of hydrogels and curing dental sealants and bone glues is existing (Benson, 2002).

A series of thiouracil complexes of Ni^{2+}, Pt^{4+}, UO_2^{2+}, VO^{2+} and Pd^{2+} of ligand (5,5-((1E,10E)-(4-chloro-1,2-phenylene) bis(diazene-2,1-diyl) bis(2-thioxo-2,3-dihydropyrimidin-4(1H)-one) was synthesized and characterized by spectroscopic techniques and different measurements. VO^{2+} complex was irradiated by using Gamma radiation to through a light on the possibility of geometry variations with the effect of radiation. The parameters exhibited from ESR spectra before and after γ-irradiation reproduce the inflexibility of the complex towards the effect. XRD patterns were displayed that importance on the nature of the particles and the purity of products. The ligand, Pt^{4+} and Pd^{2+} are originated in nanometer range.

The aim of this work is preparation and characterization of VO^{2+}, Mn^{2+}, Zn^{2+}, Ru^{3+}, Pd^{2+}, Ag^+ and Hg^{2+} complexes by using different spectral and physical tools before and after γ-irradiation. The possible antibacterial activities of ligand and its metal complexes before and after γ-irradiation were also investigated.

2. Experimental

2.1. Material and methods

All organic compounds and the solvents were purchased from Fluka or Merck, Naser City, Egypt. The metal salts $VOSO_4$· $3H_2O$, $MnSO_4$, $ZnSO_4$, $RuCl_3$·$3H_2O$, $PdCl_2$, $AgNO_3$ and $HgCl_2$ were obtained from Fluka and used for complex preparation without further purification.

2.2. Preparation of the metal complexes

The organic ligand 4-(4-chlorophenyl)-1-(2-(phenylamino) acetyl) thiosemicarbazone (**B**) was previously prepared and characterized (Samar and Ayman, 2017). Metal complexes were prepared by adding Stoichiometrical amount of MX_2· nH_2O, where M = VO^{2+}, Mn^{2+}, Zn^{2+}, Ru^{3+}, Pd^{2+}, Ag^+ and Hg^{2+} and X = SO_4^{2-} Cl^-, NO_3^- and n = 0–3 in absolute ethanol to hot solution of the ligand in (1:1) molar ratio leading to the complexes are represented in Scheme 1. The resulting mixture was magnetically stirred at 60 °C for 6–8 h. The formed precipitate was filtered off while hot, otherwise the solution was left at 35 °C to evaporate some of solvent to promote crystallization. The crystals were collected by vacuum filtrations, washed several times with anhydrous diethyl ether and dried under vacuum in presence of P_4O_{10}.

2.3. Physical measurement

Elemental analyses (C, H and N) were performed at Microanalytical unit, Cairo University. Metal content was estimated complexometric using EDTA following standard literature methods (Bassett et al., 1978). The Fourier Transform Infrared (FT-IR) measurements were performed (4000–400 cm^{-1}) in KBr discussing. Nenexeus-Nicolidite-640-MSAFT-IR, Thermo-Electronics Co. (Central Lab, Faculty of Science, Menoufia University, Egypt). ^{1}H NMR spectra was recorded in DMSO- d_6 using 300 MHz Varian NMR spectrometer (Micro Analytical Center). The UV–visible absorption spectra was measured in DMF solution (10^{-3} M) using 4802 UV/vis double beam spectrophotometer. The molar conductivity measurements were made in DMF solution (10^{-3} M) using a Tacussel conductometer type CD6N. The magnetic susceptibilities of the complexes were measured by the modified Gouy method at room temperature using Magnetic Susceptibility Johnson Matthey Balance. The effective magnetic moments were calculated using the relation $\mu_{eff} = 2.828(\chi_m T)^{1/2}$ B.M., where χ_m is the molar magnetic susceptibility corrected for diamagnetism of all atoms in the compounds using Selwood and Pascal's constants.
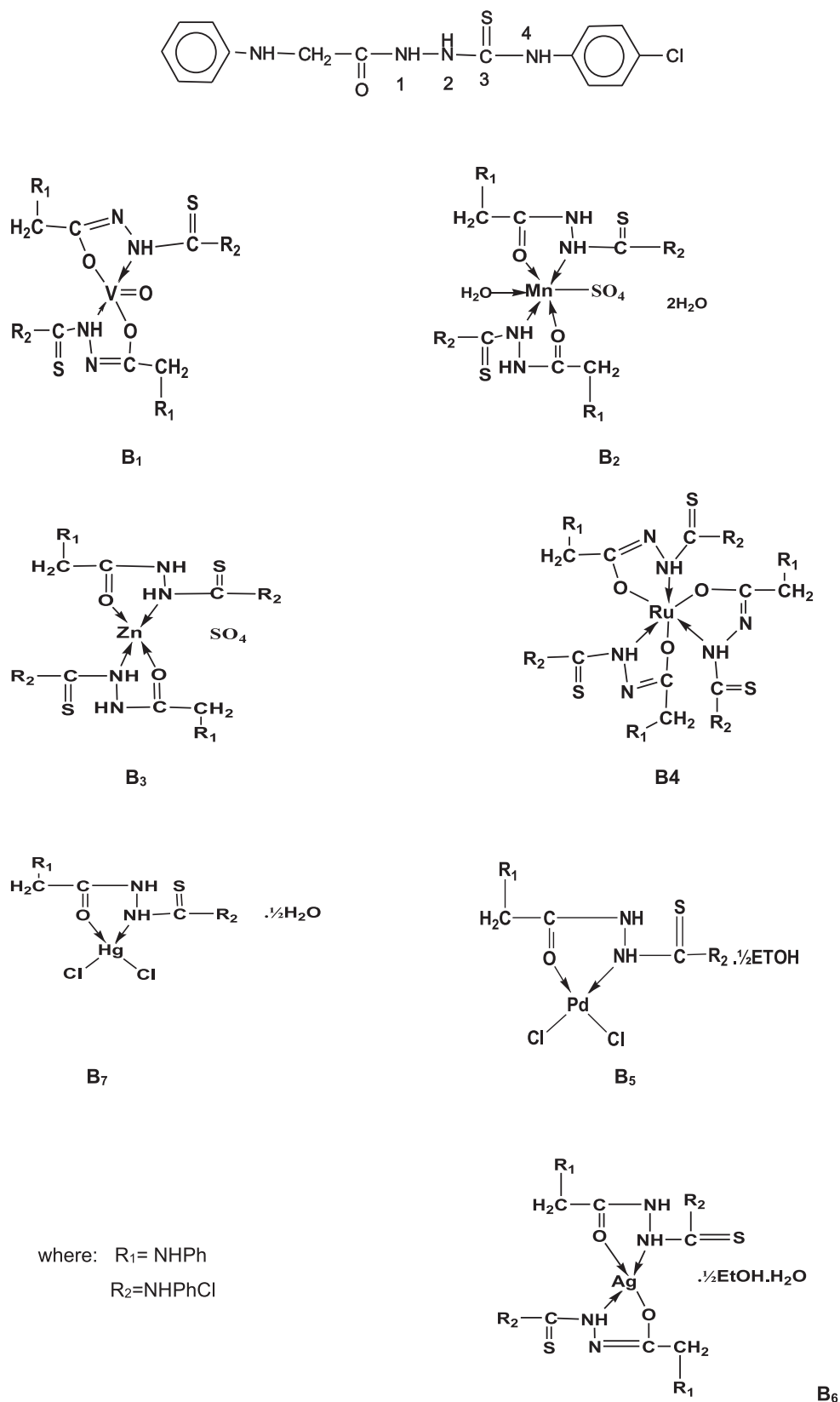
Scheme 1 Suggested chemical structures of metal complexes (B₁–B₇).

Thermal analysis (TGA/DTG) was obtained out by using a Shimadzu DTG-50 Thermal analyzer with a heating rate of 10 °C/min in nitrogen atmosphere with a following rate 20 ml/min in the temperature range 25–800 °C using platinum crucibles at Central Lab, Faculty of Science, Menoufia University, Egypt.

X-ray powder diffraction analyses of unirradiated B_2, B_5, B_6 and irradiated A_2, A_5, A_6 of solid samples were measured using Rigku Model ROTAFLEX Ru-200 at The National Research Center, Cairo, Egypt. Morphology and structural analysis by x-ray diffractograms give computer control formally finished by PHILIPS®MPDXPERT X-ray diffractometer ready with Cu radiation Cu Kα (λ = 1.540 56 Å). The x́ pert diffractometer has the Bragg- Brentano geometry. The X-ray tube was used for a copper tube operating at 40 kV and 30 mA. The scanning range (2θ) was 20–80° with step size of 0.02° and counting time of 3 s/step. Quartz was used as the standard material to accurate for the instrumental expansion. This identification of the complexes was done by a known method (Uarikumaran and Appukuttan, 2012) from the fit identified Scherrer formula, the average crystallite size, L, is

$$L = (K\lambda/\beta\cos\theta)$$

where λ is the X-ray wavelength in the manometer, K (constant equal to 0.9) is related to crystallite shape, and ß is the peak width at half maximum height. The value of ß in the 2θ axis of diffraction shape must be in radians. The θ is the Bragg angle and be able to in radians since the Cos θ compatible with the same number.

2.4. Theoretical calculation (molecular modeling)

Molecular modeling was applied to investigate the three dimensional arrangements for atoms in the complexes by employing semi-empirical molecular orbital calculations at the PM3 level provided by the HyperChem program.

2.5. Antibacterial activity

The highly pathogenic bacterium *Streptococcus pyogenes* isolated from human sources which is classified into Lancefield's group A bacteria and *E. coli* isolated from the soil of Menoufia governorate were used in this study. Brain heart infusion (BHI) broth medium (MP Bio) contained 27.5 g nutrient substrate (brain extract, heart extract and peptones), 2 g D(+) glucose, 5 g NaCl, and 2.5 g Na_2HPO_4 per liter. The pH was

adjusted to 7.4 by the addition of diluted NaOH. Nutrient broth (NB) medium contained 1 g D(+)glucose, 15 g peptone, 6 g sodium chloride, 3 g yeast extract per liter was used to grow the bacterial strains and monitoring SK activity during growth curve of the microbes. The pH was adjusted to 7.4 by the addition of diluted NaOH.

The in vitro antibacterial activities of the tested complexes were assessed as described (Hanaa et al., 2016) with some modification. The inhibitory effects of synthesized ligand and its complexes before and after exposure to γ-irradiation were tested on the pathogenic Gram-positive organism *Streptococcus pyogenes* and the Gram–negative bacterium *Escherichia coli*. Brain Heart Infusion (BHI) broth was used to grow *Streptococcus pyogenes* cells and nutrient broth medium was used to grow *E. coli* cells. Compounds were dissolved in DMSO which has no inhibition activity on both microbes. Two different concentrations (1 μg/ml, 5 μg/ml, 7 μg/ml and 10 μg/ml) were prepared. Bacterial strains were prepared by activating them on the proper broth media with shaking. The bacteria were cultured for 24 h at 37 °C in an incubator. One milliliter of the standard bacterial culture was used as inoculation in a broth medium. For growth studies, *S. pyogenes* and *E. coli* cultures were inoculated and grown aerobically on BHI broth medium and NB medium respectively. Growth was calculated turbidometrically at 650 nm using conventional spectrophotometer. After growing bacterial cultures on media that contain the ligand, the complex and the control, absorption measurements were accomplished by spectrophotometer after 24 and 48 h of incubation to determine the number of viable cells count per milliliter of sample and were used to the calculated the inhibition percentage.

2.6. Irradiation studies

For irradiation studies of solid samples of complexes B_1–B_7 were subjected to γ-irradiation to a dose of 60 kGy using Indian ^{60}Co γ-ray cell type GE-4000 A (at room temperature at the Egyptian Atomic Energy Authority Nasr City, Egypt) at a dose rate of 2.2 kGy h^{-1}. After removing the samples from the radiation field the FT-IR, absorption spectra and thermal analysis (TG/DTG) XRD, antibacterial activities of the irradiated samples were investigated. X-ray powder diffraction analyses of unirradiated B_1–B_7 and irradiated A_1–A_7 samples of complexes were carried out at the National Research center, Dokki, Cairo, Egypt by using Rigku Model ROTAFLEX Ru-200. Divergence and receiving slits were 1 and 0.1, respectively.

Table 1 Elemental analysis and molar conductivities of ligand (B) and complexes (B_1–B_7).

| No | Compound | Color | Yield% | Mol.Wt | Found (Calc) % | | | | | $^{\Lambda}$m |
					C	H	N	Cl	M	
B	H_2L	Pale brown	75	334.5	53.43(53.81)	4.46(4.48)	16.47(16.7)	10.83(10.6)	–	–
B$_1$	VO (HL)$_2$	Brown	60	733.9	49.23(49.05)	3.71(3.81)	15.52(15.26)	9.80(9.67)	6.23(6.94)	20
B$_2$	Mn (H$_2$L)$_2$SO$_4$.2H$_2$O	Brown	60	856	42.75(43.16)	3.64(3.97)	12.9 (13.08)	8.87(8.29)	6.32(6.41)	34
B$_3$	Zn (H$_2$L)$_2$SO$_4$	Pale Brown	65	830.8	43.0(43.33)	3.33(3.61)	13.36(13.4)	8.87(8.55)	7.62(7.87)	20
B$_4$	Ru(HL)$_3$	Black	75	1101.5	49.4(49.0)	3.74(3.81)	14.70(15.2)	9.60(9.96)	10.1(9.17)	35
B$_5$	Pd (H$_2$L)Cl$_2$. ½ETOH	Yellow	70	534.8	35.57(35.9)	3.12(3.36)	10.2(10.4)	20.20(19.9)	19.49(19.87)	18
B$_6$	Ag(HL)(H$_2$L). ½ETOH.H$_2$O	Brown	70	816.9	45.74(45.54)	3.94(4.16)	13.4(13.71)	8.87(8.69)	13.66(13.2)	12
B$_7$	Hg (H$_2$L)Cl$_2$. ½H$_2$O	Pale Brown	75	615.1	29.5(29.26)	2.86(2.60)	8.83(9.10)	17.57(17.3)	32.93(32.61)	20

Where:
$^{\Lambda}$ m = molar conductivity (Ω^{-1} cm^2 mol^{-1}) in 10^{-3} M DMF solution.

3. Results and discussion

3.1. Physical data

The data shows that the reactions of the ligand with oxovanadium, manganese, zinc sulfate, ruthenium, palladium, mercuric chloride and silver nitrate in 1 M:1L molar ratio are resulted in given metal complexes **B₁–B₇** (Table 1). The molar conductiv-

ities in DMF (10^{-3} M) solution exhibited that all metal complexes are non-electrolytes in nature (Geary, 1971).

3.2. Spectroscopic analysis

3.2.1. Proton nuclear magnetic resonance spectra

Comparison of the proton nuclear magnetic resonance of **B** and **A** (ligand before and after γ-irradiation) were recorded
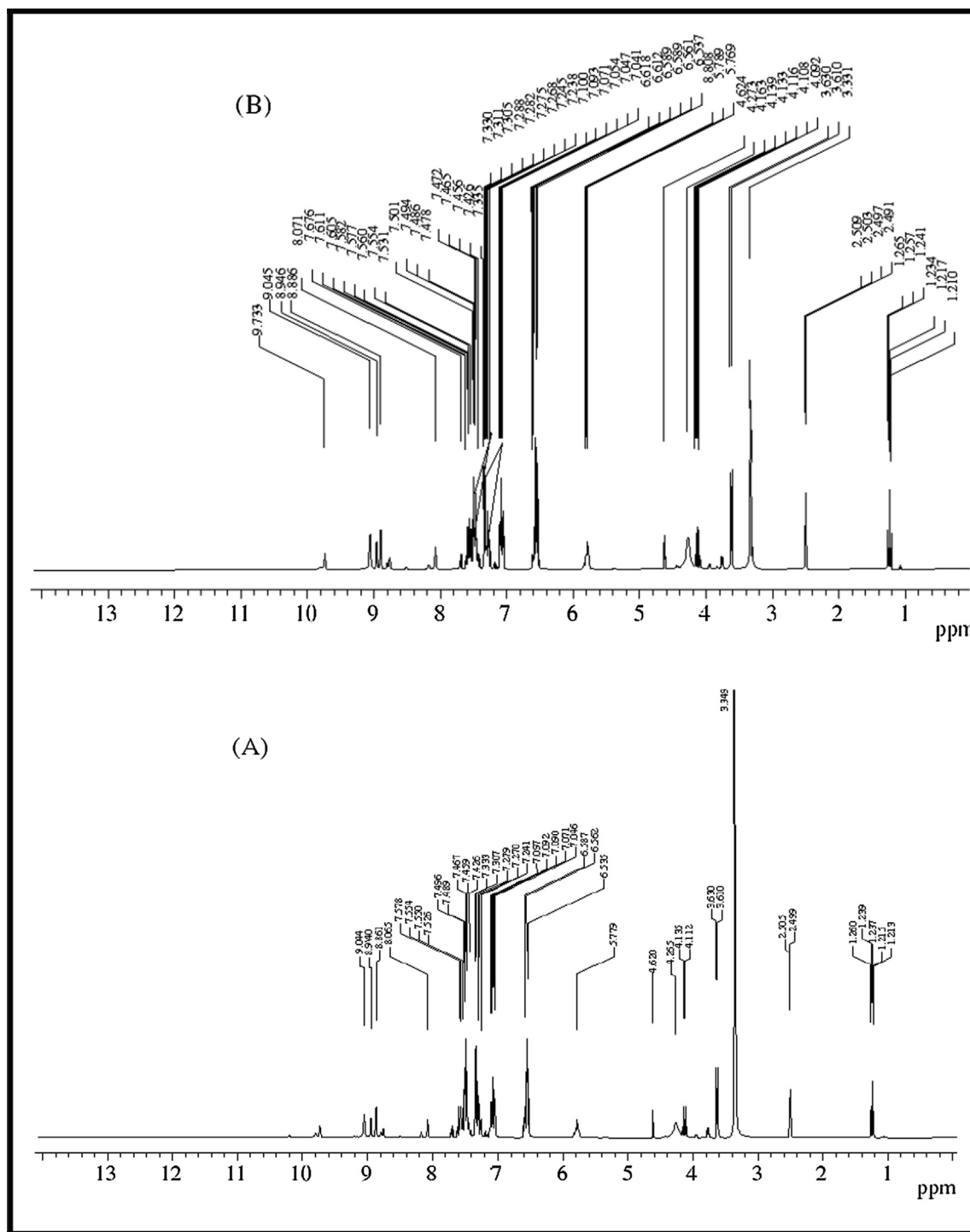
Fig. 1 ^{1}H NMR spectra of ligand in DMSO d_6 solution before and after irradiation (B, A).

in DMSO d_6 solution (Fig. 1). The ^{1}H NMR spectra of **B** and **A** in DMSO d_6 revealed a chemical shift (δ, ppm) = 2.5 ppm, the N(4)H signal appeared at 8.85, 8.07 ppm and the N(2)H signal appeared at 9.7, 9.04 ppm and the peak of N(1)H appeared at 9.04, 8.9 ppm. The singlet signal appeared at 3.3, 3.2 ppm that are attributed to the protons of CH_2, the multiplet signal appeared at 6.7–7.5, 6.8–7.4 ppm that are attributed to the aryl protons. The intensity of irradiated (**A**) is higher than unirradiated (**B**) (Samar and Ayman, 2017; Samar, 2017). Also, ^{1}H NMR spectrum of [Pd(H$_2$L)Cl$_2$]· ½ ETOH complex (Fig. 2) was recorded in DMSO d_6. After γ-irradiation the spectrum of [Pd(H$_2$L)Cl$_2$]· ½ ETOH complex showed new peaks at 8.07, 9.0, 9.2 and 9.09 ppm is attributed to N(4)H, N(2)H, N(1)H, but the signal of N(2)H in **B$_5$** is

Fig. 2 ^{1}H NMR spectra of Pd(II) complexes in DMSO d_6 solution before irradiation and after irradiation (B$_5$, A$_5$).

downfield 9.09 ppm as a comparison of **B** at 9.7 ppm. By using gamma ray the intensity of bands is higher than unirradiated

3.2.2. Mass spectroscopy

The mass spectrum of the ligand exhibited a molecular ion peak at $m/z = 336$ amu (Calc. $m/z = 334.5$). The important fragment ions appear at: m/z 77 for $[C_6H_4\text{-}3H]^+$, 112 for $[C_6H_5Cl\text{ -}H]^+$, 127 for $[C_6H_5NCl\text{- }2H]^+$, 201 for $[C_7H_9N_3\text{-}SCl]^+$, 228.5 for $[C_8H_9N_3SOCl\text{-}H]^+$, 259 for $[C_9H_{10}N_4OSCl\text{-}2H]^+$, 336 for $[C_{15}H_{15}N_4OSCl]$ (Fig. 3). Also, the spectrum of complex $[Hg(H_2L)Cl_2]\cdot\frac{1}{2} H_2O$ proceed the suggested formula by appearing a molecular ion peak at m/z 590 amu in proportion to $[Hg(H_2L)Cl_2]\cdot\frac{1}{2} H_2O]$(**B$_7$**) which agree with its formula weight (calculated $m/z = 606.1$ amu). The additional fragments of **A$_7$** and **B$_7$** provide the peaks with various intensities at diverse m/z values approximating at: Calc/Found 76/77 $[C_6H_4]^+$, 91/90 $[C_6H_4NH]^+$, 126.5/127$[C_6H_4NHCl]^+$, 327.1/327$[C_6H_4NHClHg]^+$, 362.6/361$[C_6H_4NHCl_2Hg]^+$, 398.1/398$[C_6H_4NHCl_3Hg]^+$, 498.1/498$[M\text{-}(C_9H_9N_3Cl_3HgS]^+$, 590.1/593 $[M\text{-}(C_{15}H_{15}N_4Cl_3 HgOS)]^+$, 606.1/606 $[M\text{-}\frac{1}{2}H_2O]^+$. After γ-irradiation, the molecular ions tend to be more stable and break into fragments with higher intensity than before γ-irradiation.

3.2.3. IR spectra

The most important assignments of the IR spectra of the free organic ligand and its metal complexes **B$_1$–B$_7$** and **A$_1$–A$_7$** are done in the range 4000–400 cm^{-1}. The comparison between the functional groups for unirradiated and irradiated ligand **B** and **A** is presented in Fig. 4 and Table 2. It was found that the functional groups of the ligand **B** appear at 3302; 3302 cm^{-1}, 3100; 3103 cm^{-1}, 1670; 1668 cm^{-1} and 750; 751 cm^{-1} respectively are attributed to the stretching frequencies of υ(N2—H), υ(N1—H), υ(C=O) and υ(C=S), respectively. After γ-irradiation their corresponding bands υ(N1—H) and υ(C=S) were shifted to higher wave numbers as compared to that of free B. While, the functional group of υ(C=O) shifted to lower wave number after γ-irradiation) (Morsy et al., 2011). After γ-irradiation the intensity of the peaks become more sharper than that of unirradiated ligand.

Coordination modes of respective unirradiated **B$_1$–B$_7$** and irradiated metal complexes **A$_1$–A$_7$** have been proven by comparing with ligand **B**. VO(II) and Ru(III) complexes **B$_1$**, **B$_4$**, and **A$_1$**, **A$_4$** are shown significant changes showed significant changes compared to the spectrum of free **B**. The most important diagnostic spectral bands are exhibited at 3358–3296, 3233–3101 and 758–755 cm^{-1} in **B$_1$**, **B$_4$**. Also, the IR spectra
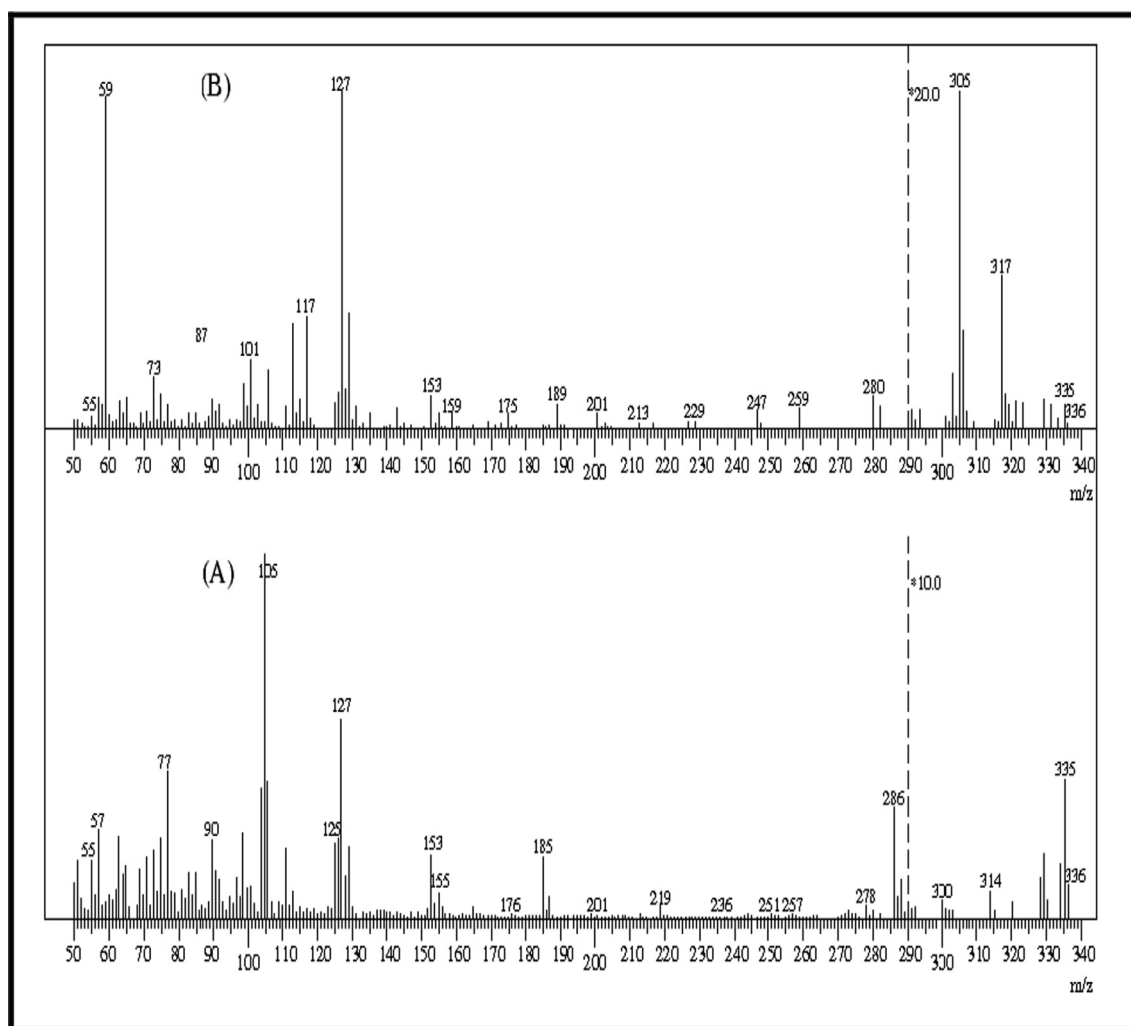
Fig. 3 Mass spectra of ligand before and after irradiation (B, A).
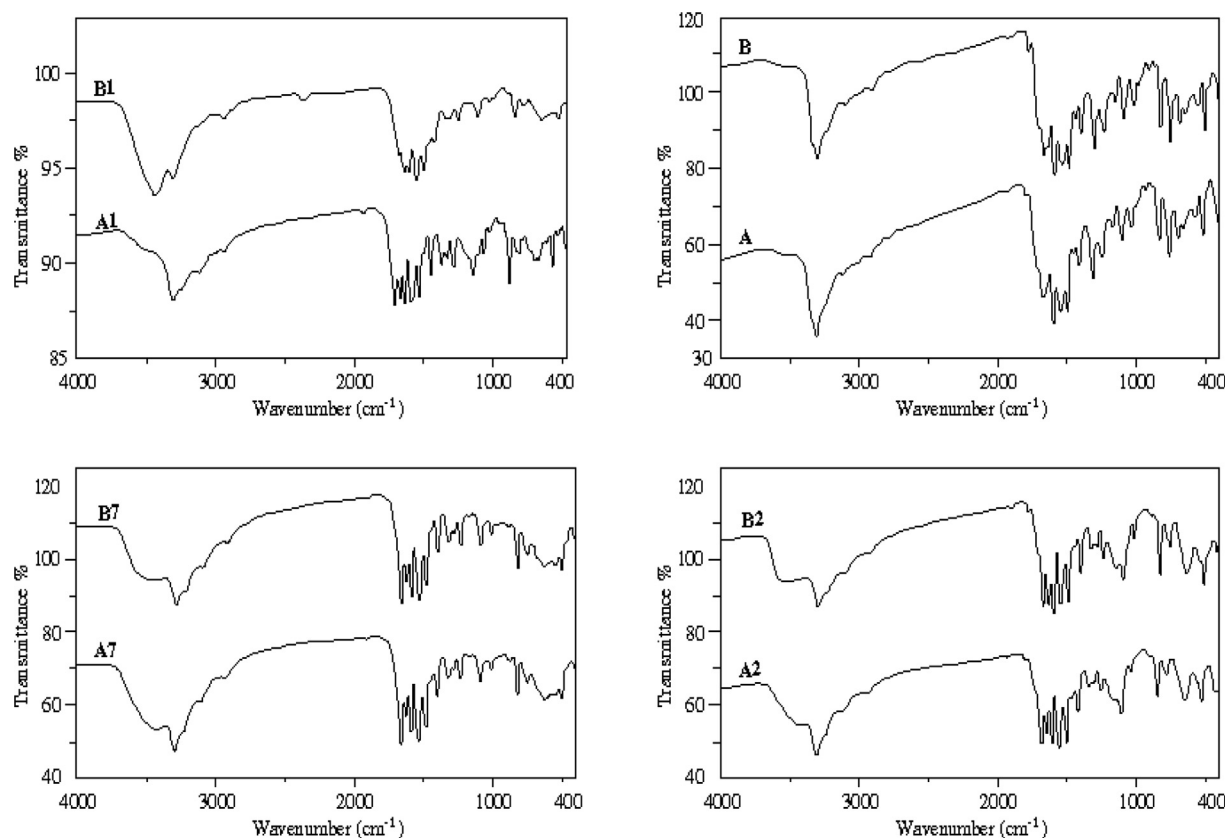
Fig. 4 IR spectra of ligand and VO(II), Mn(II), Hg(II) complexes before and after irradiation (B, B$_1$, B$_2$, B$_7$ and A, A$_1$, A$_2$, A$_7$).

Table 2 Infrared spectral bands (cm^{-1}) for ligand and its metal complexes.

	Compound	v(N4—H)	v(N2—H)	v(N1—H)	v(C=O)	v(C=S)	v(M—N)	v(M—O)
B	H$_2$L	3335	3302	3100	1670	750	–	–
A	H$_2$L	3481	3302	3103	1668	751	–	–
B$_1$	VO(HL)$_2$	3430	3358	3301	–	758	509	634
A$_1$	VO(HL)$_2$	3422	3295	3233	–	757	467	636
B$_2$	Mn(H$_2$L)$_2$SO$_4$·2H$_2$O	3502	3296	3101	1672	753	436	634.5
A$_2$	Mn(H$_2$L)$_2$SO$_4$·2H$_2$O	3408	3296	2927	1672	755	508	633.5
B$_3$	Zn(H$_2$L)$_2$SO4	3499	3296	3102	1631	725	467	635
A$_3$	Zn(H$_2$L)$_2$SO4	3470	3296	3104	1632	756	468	635
B$_4$	Ru(HL)$_3$	3450	3296	3101	–	756	468	638
A$_4$	Ru(HL)$_3$	3480	3296	3101	–	755	465	638
B$_5$	Pd(H$_2$L)Cl$_2$·½ETOH	3444	3296	3197	1602	760	457	601
A$_5$	Pd(H$_2$L)Cl$_2$·½ETOH	3424	3296	3196	1603	761	465	603
B$_6$	Ag(H$_2$L)(HL)H$_2$O·½ETOH	3428	3296	3100	1633	753	549	409
A$_6$	Ag(H$_2$L)(HL)H$_2$O·½ETOH	3430	3295	3100	1633	753	507	413
B$_7$	Hg (H$_2$L)Cl$_2$·½H$_2$O	3465	3297(m)	3104	1632	755	509	550
A$_7$	Hg (H$_2$L)Cl$_2$·½H$_2$O	3420	3296	2926	1633	755	509	555

Where:
B = before γ-irradiation.
A = after γ-irradiation.

of **A$_1$**, **A$_4$** are showed bands at 3233–3101 and 757–756 cm^{-1}, respectively, which attributed to the stretching frequencies of υ(N2—H), υ(N1—H) and υ(C=S). The bands corresponding to υ(N2—H), υ(C=S) were shifted to lower frequency of complexes **A$_1$** and **A$_4$**. However, the IR spectra of VO(II) and Ru(III) complexes before and after γ-irradiation were showed

that υ(C=O) disappeared upon complexes formation, indicating the coordination of the ligand in enol-form and the ligand behaves as monobasic tetradentate. Also, coordination takes place via N(2)H and enolic oxygen (C—O). On the other side, IR spectra (Fig. 4) of complexes before **B$_2$**, **B$_3$**, **B$_5$**, **B$_6$** and **B$_7$** and after γ-irradiation **A$_2$**, **A$_3$**, **A$_5$**, **A$_6$** and **A$_7$** show four strong

bands at 3296; 3100–3197; 1601–1672 and 725–760 respectively, also bands at 3101–3295; 3297–3196; 1601–1672 and 753–761 cm^{-1}, respectively that are attributed to υ(N4—H), υ (N2—H), υ(N1—H), υ(C=O) and υ(C=S). After γ- irradiation, the bands corresponding to υ(N1—H) was shifted to lower frequency as compared to those of complexes B_2, B_5 and B_7. However, the band attributed to υ(C=S) was shifted to higher wave number and higher intensity of band of irradiated. While, in complexes A_4 and A_6 the υ(C=O) is shifted to higher wave number as compared to that unirradiated complexes. The new bands appeared at 638–549; 638–507, 509–409 and 508–413 cm^{-1} are assigned to υ(M—O) and υ(M—N) for B_1–B_7 and A_1–A_7 complexes, respectively (Krishnan et al., 2010; Seena and Kurup, 2007). The IR spectra of VO (II) complexes before and after γ-irradiation display new bands at 1012 and 1014 cm^{-1} assigned to υ(V=O) (Maany et al., 2006).

3.2.4. Electronic spectra and magnetic measurements

The electronic spectral bands of the ligand **B**, irradiated **A** and complexes B_1–B_7 and irradiated complexes A_1–A_7 (λ_{max}, nm) in DMF solution and (μ_{eff} B.M.) are measured. UV/vis spectra of complexes B_1 and A_1 exhibit one band at 600 and 620 nm. The observed bands are assigned to $^2B_2 \rightarrow {}^2E$ electronic transition suggesting a square pyramidal geometry around VO^{2+} ion. The magnetic moment values are found to be 1.56 B.M and 1.57 B.M. for B_1 and A_1 which is an indicative of square pyramidal geometry) (Adly, 2011).

The electronic spectra of zinc complexes B_2 and A_2 display two bands at 320 nm and 340 nm which may be attributed to π-π^* and n-π^* transitions, respectively. The Zn^{2+} complexes show no d-d band. The coordination of the sulfate ion to the tetrahedral zinc center is proved by its non-electrolytic character in dimethyl formamide solution. The electronic spectrum exhibits tetrahedral structure around the Zn^{2+} ion which is
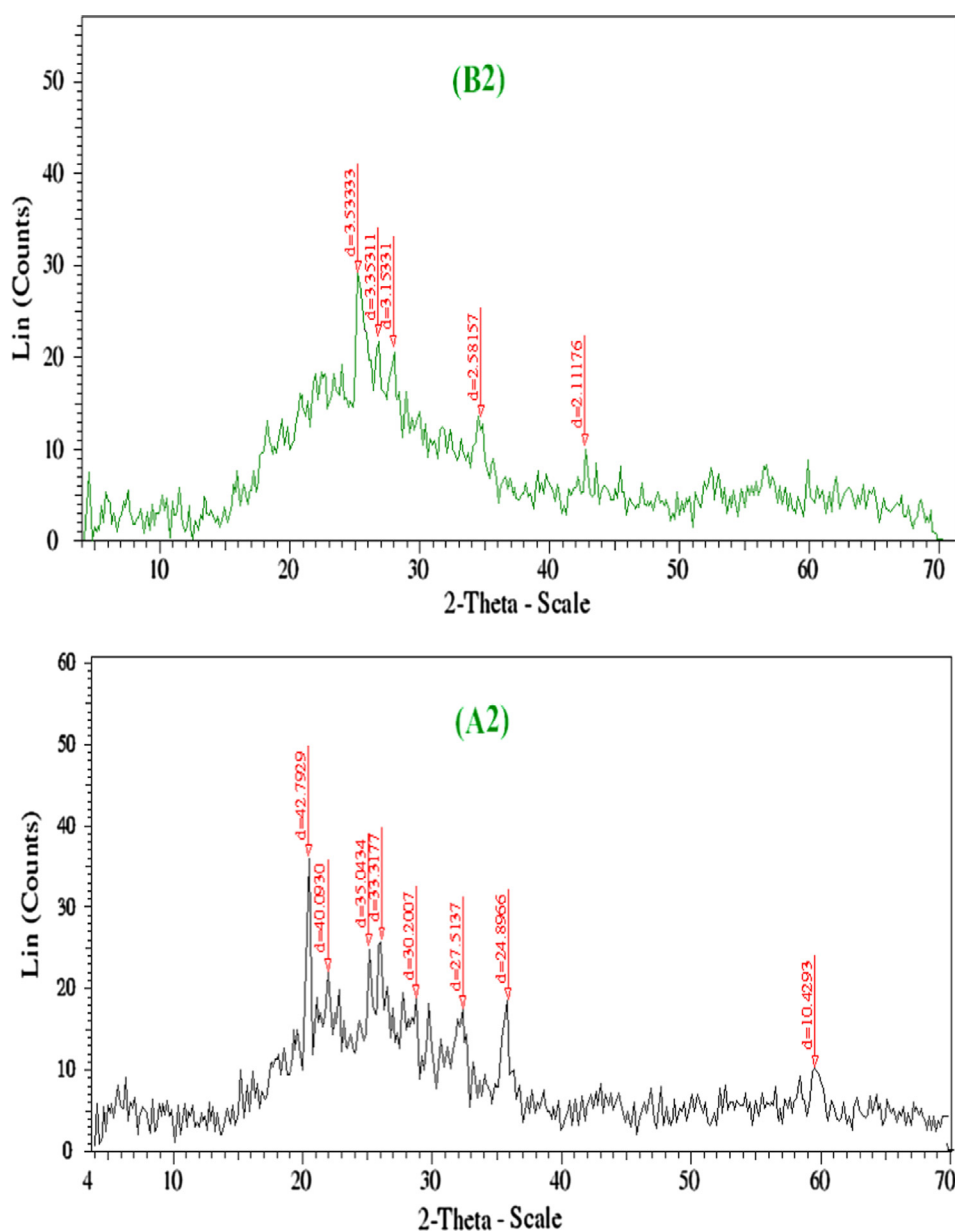
Fig. 5a   XRD spectra of Mn(II) complexes before and after irradiation (B$_2$ and A$_2$).

additional proved by its diamagnetic character (Singh et al., 2014; Raja and Ramesh, 2010).

Ru^{3+} and Mn^{2+} complexes before and after γ-irradiation B_2, B_4 and A_2, A_4 show bands at 500; 550 and 320, 330; 340 nm are assigned to $^2T_{2g} \rightarrow {}^4T_{1g}$ transition and $^6A_{1g} \rightarrow {}^4T_{1g}$, $^6A_{1g} \rightarrow {}^4E_g$ and $^6A1_g \rightarrow {}^4T_{1g}$ electronic transition respectively suggesting octahedral geometry around M$^{3+,2+}$ ion (Raja and Ramesh, 2010; Chandra and Kumar, 2005). The magnetic susceptibility measurements are found to be (1.54 and 5.4, 6.1 B.M.) for B_4, A_4 and B_2, A_2 (Hanaa and Ocala, 2015).

Pd^{2+}, Ag$^+$ and Hg^{2+} complexes before γ-irradiation B_5, B_6, B_7 and A_5, A_6, A_7 give three, two and one bands at 600, 450, 420; 360, 240; 340 nm. While electronic spectra of the complexes A_5, A_6 and A_7 after γ-irradiation appear bands at 620, 450; 380, 300, and 360 nm attributed to $^1A_{1g} \rightarrow {}^1A_{2g}$,

$^1A_{1g} \rightarrow {}^1B_{1g}$ and $^1A_{1g} \rightarrow {}^1E_g$ transitions in B_5 and A_5 (Geeta et al., 2010) intra ligand and charge transfer transitions. Diamagnetic behavior and molar conductance value confirming the square planar geometry of B_5, B_6 and B_7 (Piyali et al., 2015; Nabil and Hegab, 2005; Aliakbar et al., 2017; Elena et al., 2001; Nadia et al., 2017; Jeragh and El-Asmy, 2014).

The spectral bands of the complexes confirmed some better determined in structures with an amazingly higher absorbance by using radiation and no change in the geometry of metal complexes

3.3. X-ray diffraction patterns

XRD analysis was performed for the solid samples of Mn^{2+}, Pd^{2+}, Ag$^+$ B_2, B_5, B_6 and A_2, A_5, A_6 to confirm the crystal
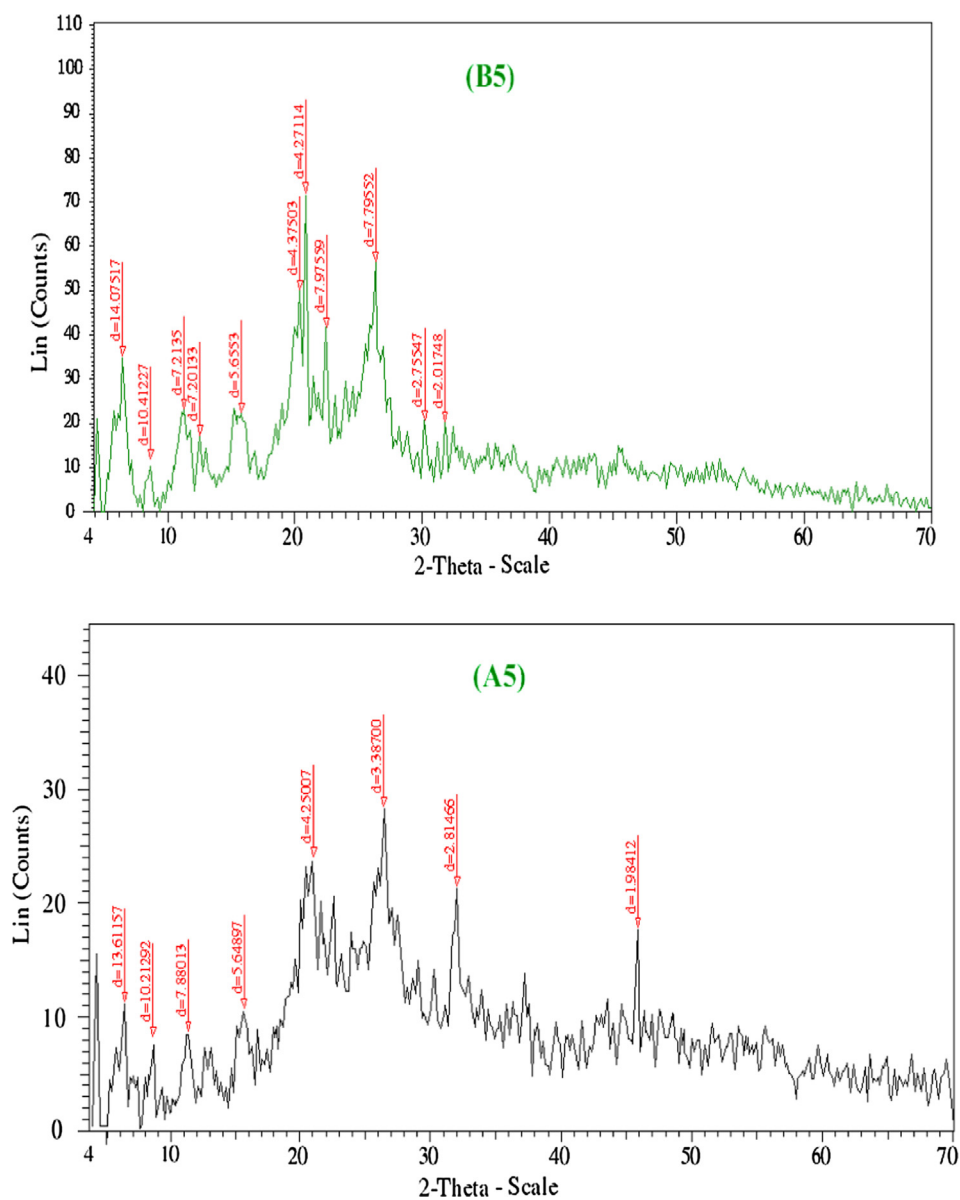
Fig. 5b   XRD spectra of Pd(II) complexes before and after irradiation (B$_5$ and A$_5$).

structure of these complexes. The XRD patterns of the created complexes were approved in order to provide insight about the lattice parameters of the prepared complexes.

Figs. 5a–5c represents XRD patterns for complexes Mn^{2+}, Pd^{2+}, Ag^+. The observed peak sharpness in the diffraction pattern indicates that Mn^{2+}, Pd^{2+}, Ag^+ complexes are in the nanometer range. The diameter of particles are found in nanorange as fellow: Mn^{2+}, 3–130 nm; Pd^{2+}, 3–172 nm; Ag^+, 3–151 nm. The nanoparticles size of complexes may serve strongly in different application fields in between the biological one (Uarikumaran and Appukuttan, 2012). The X-ray diffraction patterns of uniradiated and irradiated complexes demonstrate that:

(a) The characteristics of the material is developed
(b) Dislocation of longer interplanar spacing.
(c) New peaks appeared

As shown in Figs. 5a–5c, complexes of Mn^{2+}, Pd^{2+}, Ag^{2+} showed new peaks and some of them displaced to longer interplanar spacings. After irradiation, the position of atoms in the lattice changes and consequently, the scattering power also changed, leading to changes in intensity which exhibited a high intensity (Jayashri et al., 2014). It is noted that the effect of γ-irradiation caused a noticeable transform in the intensity of the peaks. In fact, the intensity of the peaks of irradiated is sharper than unirradiated.
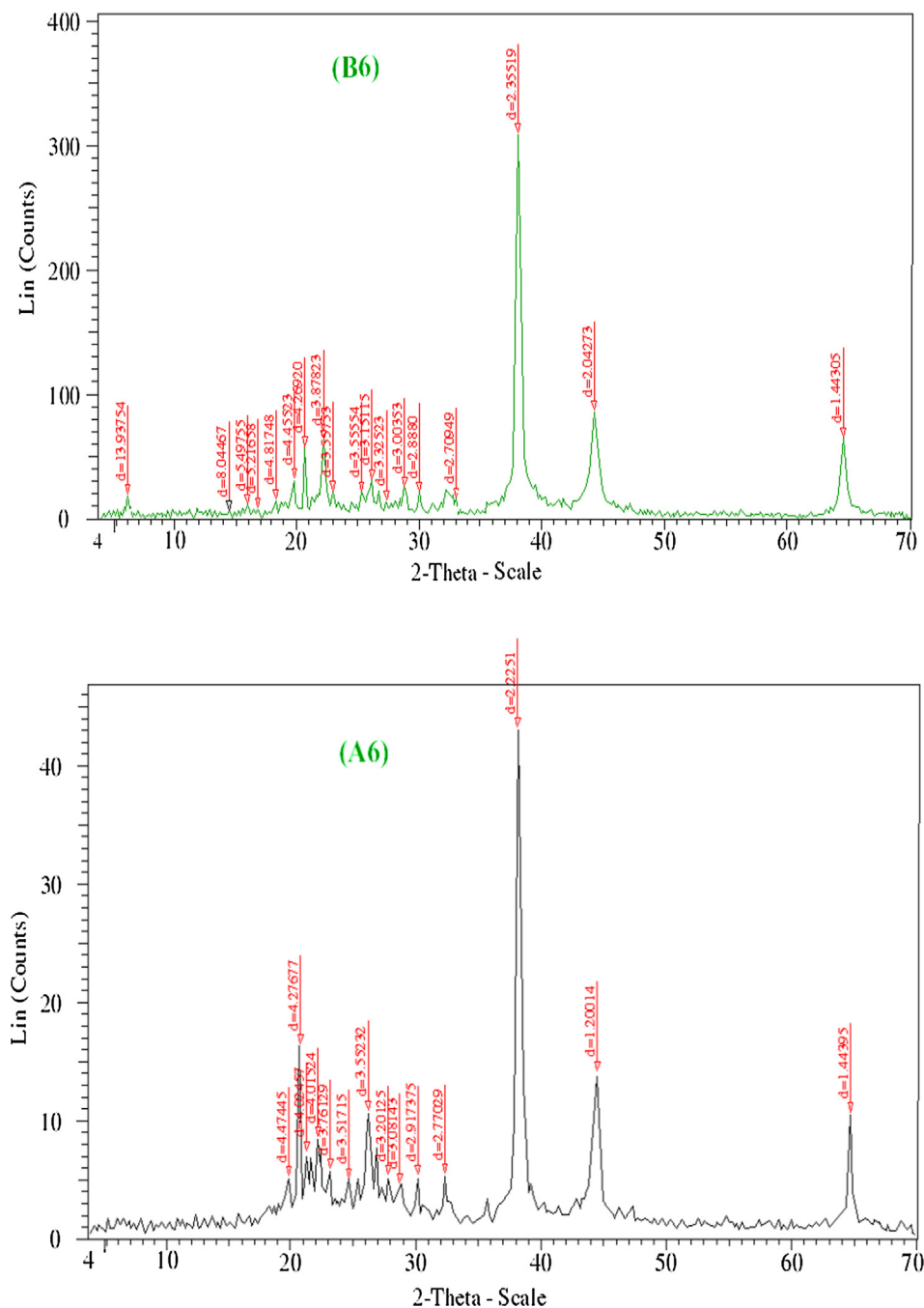
Fig. 5c   XRD spectra of Ag(I) complexes before and after irradiation (B₆ and A₆).

3.4. Thermal studies (TGA/DTG)

The thermal behavior of the **B** and its previously synthesized **B₁–B₇** complexes and **A₁–A₇** are listed in Table 3 and Figs. 6a–6d. The thermal behaviors of the ligands and their complexes **B₁–B₇** and **A₁–A₇** were investigated by thermogravimetric studies in temperature range 25–800 °C. The character of anticipated chemical change with temperature and percent of metal oxide achieved is summarized in Table 3.

The TG curve of **B** and **A** (Fig. 6a) showed a thermal stability till 150 °C and also showed two decomposition steps in the temperature range 150–633 °C; 155–680 °C with total weight loss of calc 99.9% (Found 100%); calc100% (Found

100%) before and after γ-irradiation, respectively. After γ-irradiation, the thermogravimetric analyses curves of the ligand revealed that γ-irradiation persuaded thermal stability to the substance than that of unirradiated. These results coincide well with the structure of the ligand resolute from elemental analysis and IR spectrum.

The TG curve of VO²⁺ complexes **B₁** and **A₁** (Table 3) exhibited a gradual decomposition at a temperature range 195–570 °C, leaving VO as ending remainder at 570 °C. The TG curve after γ-irradiation is similar to that of before irradiation

TGA curve for **B₂** and **A₂** exhibited three degradation stages before and after γ-irradiation (Fig. 6b). TG curves of **B₂** exhibited weight loss in the temperature range 30–100 °C

Table 3 Thermal data of the ligand and its metal complexes.

No.	Compound	TAG(A)/°C	Wt. loss Calc. (Found) %	Reaction	Leaving species
B	H₂L	At 190	–	–	Melting
		190–633	99.9	d	Gradaual decomp
A	H₂L	At 190	–	–	melting
		240–680	100	d	Gradaual decomp
B₁	VO(HL)₂	210–570	86(84.02)	d	Completion of decomp
		At 750	14.02(15.98)		VO + 3C
A₁	VO(HL)₂	210–570	86(84.02)	d	Completion of decomp
		At 750	14.02(15.98)		VO + 3C
B₂	Mn(H₂L) SO₄·2H₂O	30–279	4.2(4.9)	a	-2H₂O
		279–719	82(81.4)	d	Completion of decomp
		At 798	13.8(13.7)		MnO + 3C
A₂	Mn(H₂L) SO₄·2H₂O	30–279	4.2(4.9)	a	-2H₂O
		279–719	83.4(81.4)	d	Completion of decomp
		At 798	12.48(13.7)		MnO + 3C
B₃	Zn(H₂L)₂SO₄	395–719	87.4(86.22)	d	Completion of decomp
		At 798	12.6(13.78)		ZnO + 2C
A₃	Zn(H₂L)₂SO₄	395–719	87.4(86.22)	d	Completion of decomp
		At 798	12.6(13.78)		ZnO + 2C
B₄	Ru(HL)₃	210–389	87.9(88.7)	d	Completion of decomp.
		389–688	12.07(12.1)		RuO₂
A₄	Ru(HL)₃	180–493	77.3(79.5)	d	Completion of decomp.
		493–680	22.6(20.5)		Ru₂O₃
B₅	Pd(H₂L)Cl₂·½ETOH	30–196	4.3(4.9)	b	−½EtOH
		196–383	70 (70.67)	d	Completion of decomp.
		At 561	24.9(25.02)		PdO + C
A₅	Pd(H₂L)Cl₂·½ETOH	30–200	4.9(4.3)	b	-½EtOH
		200–332	77.2 (75.9)	d	Completion of decomp
		At 699	17.9(19.8)		Pd
B₆	Ag(HL)(H₂L)·½ETOH·H₂O	30–113	5.1(7.03)	a + b	-½ETOH + H₂O
		390–642	87.49(86)	d	Completion of decomp
		At 799	7.5(6.96)		½AgO
A₆	Ag(HL)(H₂L)·½ETOH·H₂O	30–113	5.1(7.03)	a + b	-½ETOH + H₂O
		390–642	87.49(86)	d	Completion of decomp
		At 799	7.5(6.96)		½AgO
B₇	Hg (H₂L)Cl₂·½H₂O	30–100	1.4(1.39)	a	-½H₂O
		395–615	81(79.9)	d	Completion of decomp
		At 799	17.6(18.7)		½HgO
A₇	Hg (H₂L)Cl₂·½H₂O	30–100	1.4(1.39)	a	½H₂O
		395–615	81(79.9)	d	Completion of decomp
		At 799	17.6(18.7)		½HgO

[a] Dehydration.
[b] Desolvation.
[c] Final product percent.
[d] Decomposition.
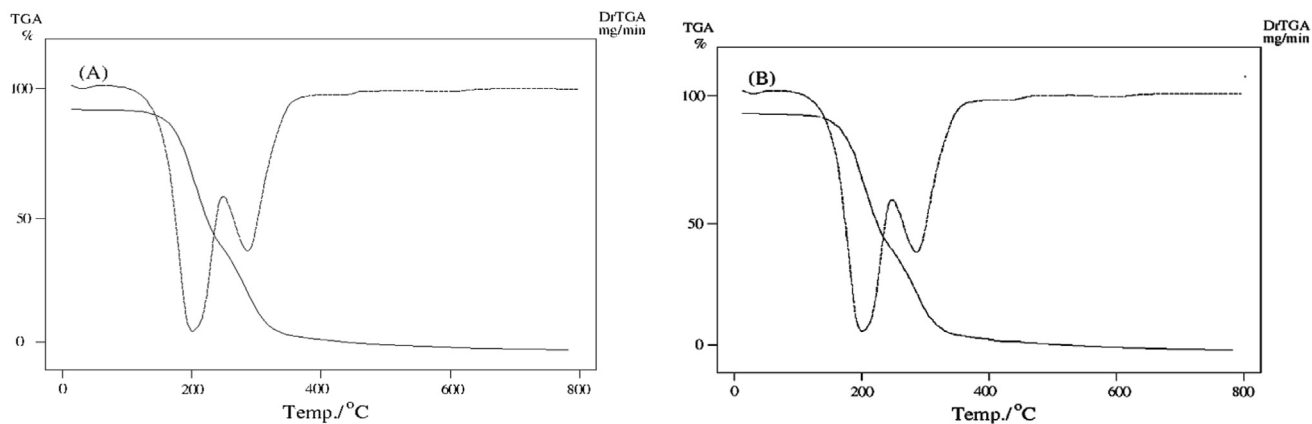
Fig. 6a TGA/DTG curves of ligand before and after irradiation (B and A).
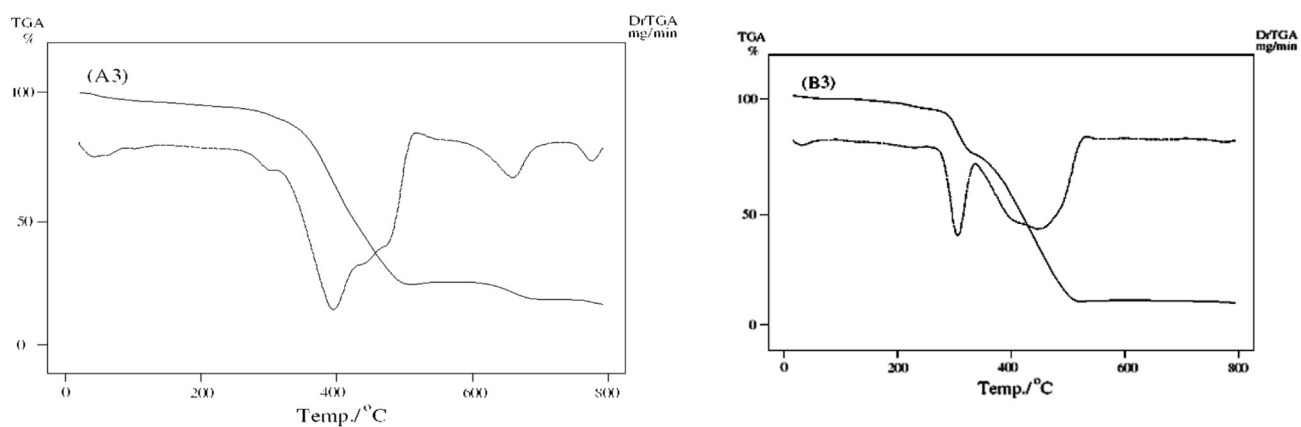
Fig. 6b TGA/DTG curves of unirradiated (B_3) and irradiated (A_3).
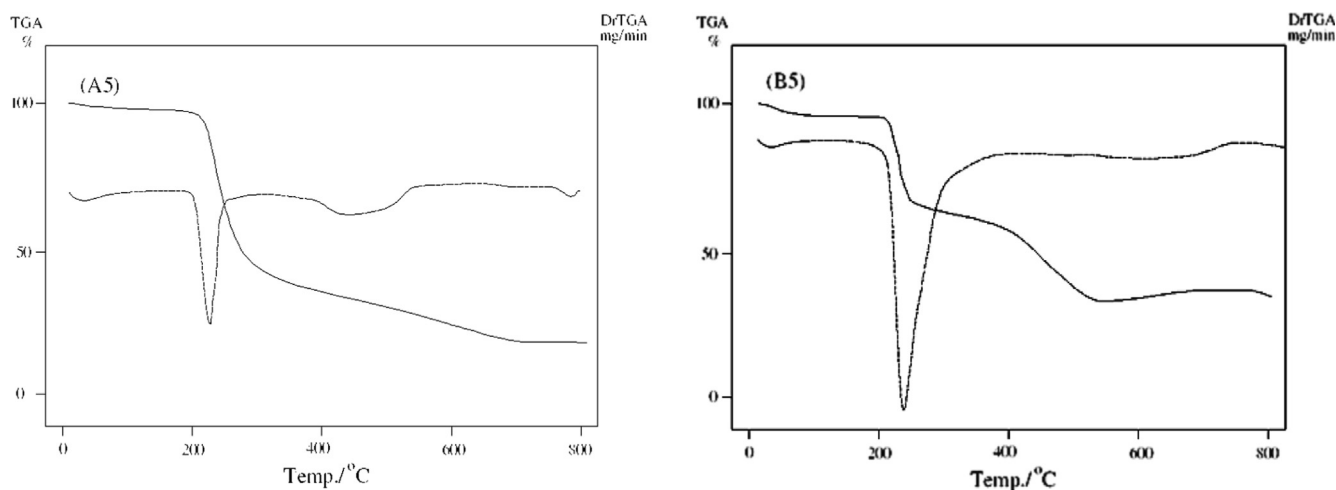
Fig. 6c TGA/DTG curves of unirradiated (B_5) and irradiated (A_5).

(Calc./Found % 4.2/4.9 that was allocated to loss of two molecules of water. The TG curve showed gradual decomposition at a temperature range 279–490 °C, leaving MnO as final remainder at 798 °C. The TG curve after γ-irradiation is similar to that of before irradiation

As shown in Fig. 6c, TGA curve of Zn^{2+} complexes B_3 and A_3 illustrated the first stage at temperature range 233–719 °C and second stage ended with leaving ZnO as final residue at 798 °C. The TG curve after irradiation of complex A_3 reveals no change as compared to B_3 before irradiation.
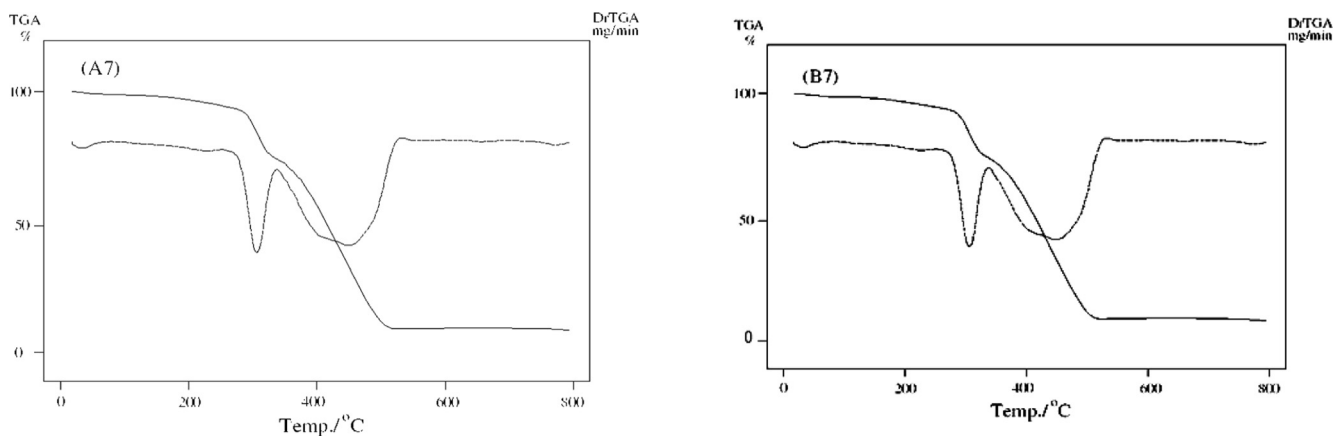
Fig. 6d   TGA/DTG curves of unirradiated (B$_7$) and irradiated (A$_7$).

The TG curve of Ru^{3+} complexes exhibited two degradation stages before and after γ-irradiation (Table 3). For **B$_4$**, the first stage starts at temperature range 150–389 °C, and the second stage ended with leaving RuO$_2$ as final residue at 688 °C. For **A$_4$**, the TG curve showed a gradual decomposition at a temperature range 180–493 °C, leaving Ru$_2$O$_3$ as ending remains at 680 °C.

Pd^{2+} complexes **B$_5$** and **A$_5$** demonstrated weight loss in the temperature range 30–196 °C (Calc./Found % 4.3/4.9) that was assigned to loss of half ethanol molecule. The TG curve revealed gradual decomposition at a temperature range 196–383 °C, leaving PdO as final residue at 561 °C. But in case of **A$_5$**, the TG curve of demonstrated weight loss in the temperature range 30–200 °C (Calc./Found% 4.3/4.9) that was assigned to loss of half molecule of ethanol (Figs. 6a–6d). The TG curve displayed steady rotting at a temperature range 200–332 °C, leaving Pd as final remainder at 699 °C.

The TG curve of Ag$^+$ complexes before and after γ-irradiation **B$_6$** and **A$_6$** showed weight loss of (Calc./Found% 5.01/7.03) at temperature range 30–113 °C, that was assigned to loss of molecule of water and half molecule of ethanol (Table 3). On additional heating of **B$_6$** and **A$_6$** decomposed at 185–642 °C. The thermogram of complex illustrated one step of decomposition at 279 °C includes the completion of the decomposition process. The TG curve of **A$_6$** after γ-irradiation is similar to that of **B$_6$** before γ-irradiation.

Hg^{2+} complexes before and after γ-irradiation **B$_7$** and **A$_7$** displayed three degradation stages (Fig. 6d). The first stage of **B$_7$** exhibited weight loss in the temperature range 30–100 °C (Calc./Found% 1.4/1.39) that was assigned to loss of half molecule of water. The second stage exhibited a gradual decomposition at a temperature range 255–615 °C. The final stage at 799 °C assigned to leave half molecule of HgO. After γ- irradiation, the TG curve of **A$_7$** is similar to **B$_7$** before γ-irradiation.

It is noted that the slightly higher value produced for the percentage of the remainder when relative to the theoretical value of pure metal oxide in **B$_1$**, **A$_1$**, **B$_2$**, **A$_2$**, **B$_3$**, **A$_3$** and **B$_5$** exhibited that the remains were impure with carbon. The character of the remains was accounted and recognized by infrared spectroscopy (Ahmed, 2006; Sanaa et al., 2015).

3.5. Molecular modeling

Molecular modeling was applied to investigate the three-dimensional arrangements of atoms in the chelates by employing semi-empirical molecular orbital calculations at the PM3 level provided by the Hyperchem 8.03 program (HyperChem, 2007).

Several shots to develop suitable crystals for X-ray crystallography were ineffective. Using theoretical parameters helps to characterize the molecular structure of the investigated com-
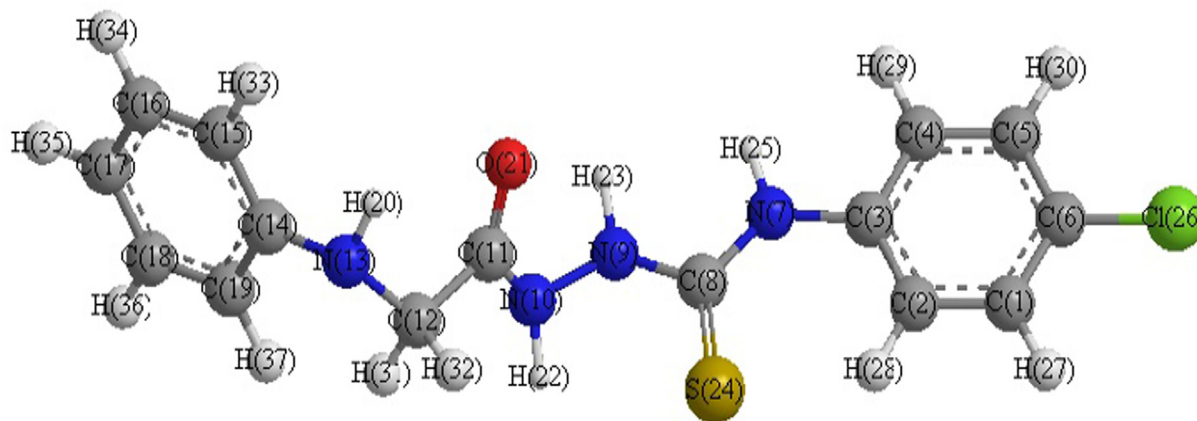
Fig. 7a   Optimized molecular structure of ligand (B).
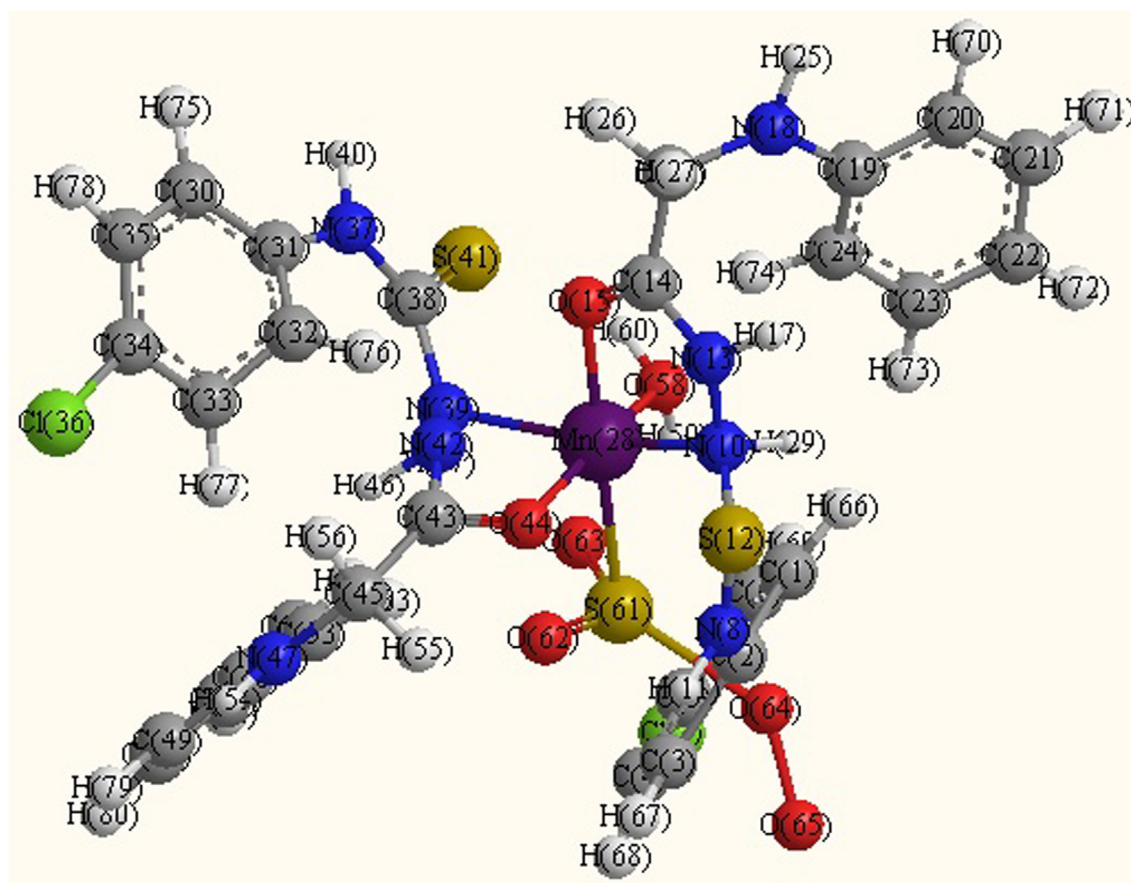
Fig. 7b Optimized molecular structure Mn complex (B_2).

plexes. Thus, the geometries of the ligand, Mn^{2+}, Pd^{2+} and Hg^{2+} complexes were optimized by hyper chem. 8.03 Molecular Modeling and Analysis Program (Mohamed et al., 2015) using the molecular mechanics calculations (PM3). The calculated bond lengths and bond angles for the **B**, **B₂**, **B₅** and **B₇** complexes are listed in tables (S1–S4).

The energetic properties of these compounds are listed in Table 5. The optimized constructions of the ligand and **B₂**, **B₅** and **B₇** are shown in Figs. 7a, b and 8a, b. The main selected bond lengths demonstrated in Table 4 elicited the following:

- The obtained bond lengths of the N—N and C—OH groups for the ligand were 1.4320 and 1.2198 Å, respectively. The bond lengths of these groups appeared within the range 1.3246–1.5418 and 1.2056–1.3351 Å in the complexes which confirmed the coordination of these groups to the metal ions. The M—O bond length is found to be shorter than the M—N bond length, except for Pd complex.
- The values of bond angle confirmed the octahedral geometry for **B₂** and square planer for **B₅** and **B₇** complexes (Mohamed et al., 2015). The compound with higher HOMO energy implies that the molecule is a superior electron donor.
- The lower HOMO energy values illustrate that molecule donating electron aptitude is the weaker. On contrary, the LUMO energy presents the ability of a molecule receiving electron (Yousef et al., 2012; Seda et al., 2009). The energies of the HOMO and LUMO are negative which showed that the compounds under investigation were stable.

3.6. Antibacterial activity

The synthesized ligand and its metal complexes before and after γ-irradiation were tested for their potential antibacterial activities (Tweedy, 1964). Results in Tables 6 and 7 and Figs. 9 and 10 illustrated antibacterial activities against the experienced bacteria. It was established that antibacterial activities of the artificial compounds before and after γ-irradiation were
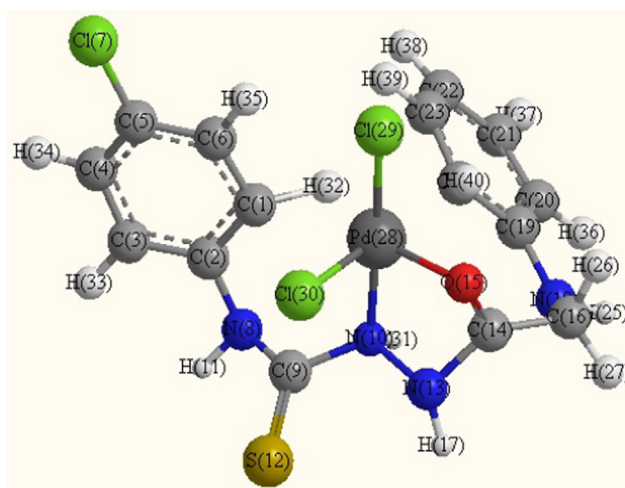
Fig. 8a Optimized molecular structure of Pdomplex (B_5).
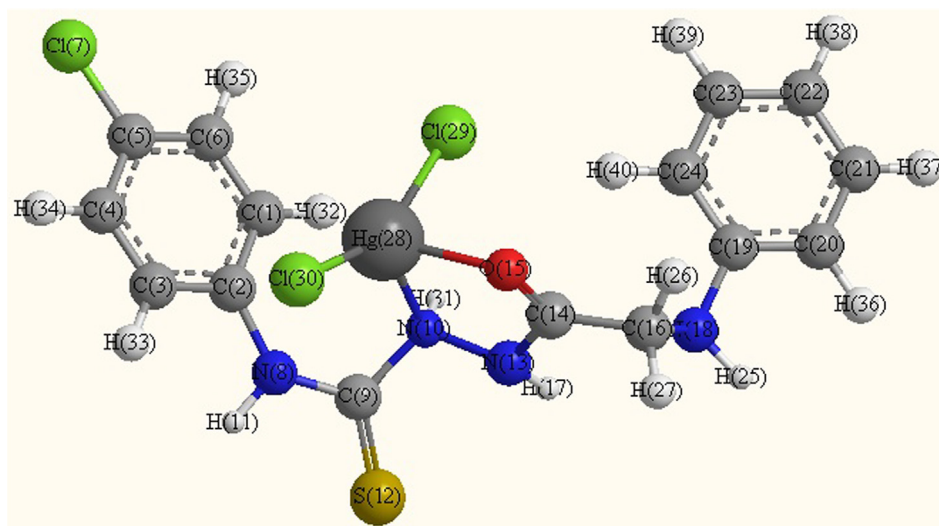
Fig. 8b Optimized molecular structure of Hg complex (B$_7$).

Table S1 Selected bond lengths (Å) and angels (°) of the ligand (B).

Ligand (B)			
Bond length		Bond angles	
C(18) —C(19)	1.3884	C(18) —C(19) —C(14)	119.9606
C(17) —C(18)	1.3913	C(19) —C(18) —C(17)	120.3044
C(16) —C(17)	1.3913	C(18) —C(17) —C(16)	119.8587
C(15) —C(16)	1.3894	C(17) —C(16) —C(15)	120.4912
C(14) —C(19)	1.4016	C(16) —C(15) —C(14)	119.7169
C(14) —C(15)	1.4020	C(19) —C(14) —C(15)	119.6678
N(13) —C(14)	1.4412	C(19) —C(14) —N(13)	120.6384
C(12) —N(13)	1.4753	C(15) —C(14) —N(13)	119.4998
C(11) —O(21)	1.2198	C(14) —N(13) —C(12)	116.9405
C(11) —C(12)	1.5197	N(13) —C(12) —C(11)	114.9431
N(10) —C(11)	1.4462	O(21) —C(11) —C(12)	125.1036
N(9) —N(10)	1.4320	O(21) —C(11) —N(10)	118.4499
C(8) —S(24)	1.6585	C(12) —C(11) —N(10)	116.3376
C(8) —N(9)	1.4463	C(11) —N(10) —N(9)	119.2792
N(7) —C(8)	1.3841	N(10) —N(9) —C(8)	119.6348
C(6) —Cl(26)	1.6819	S(24) —C(8) —N(9)	120.7164
C(5) —C(6)	1.3958	S(24) —C(8) —N(7)	128.3888
C(4) —C(5)	1.3864	N(9) —C(8) —N(7)	110.6920
C(3) —N(7)	1.4378	C(8) —N(7) —C(3)	129.2920
C(3) —C(4)	1.4085	Cl(26) —C(6) —C(5)	119.5073
C(2) —C(3)	1.4000	Cl(26) —C(6) —C(1)	119.8414
C(1) —C(6)	1.3922	C(5) —C(6) —C(1)	120.6513
C(1) —C(2)	1.3909	C(6) —C(5) —C(4)	119.6804
		C(5) —C(4) —C(3)	119.9811
		N(7) —C(3) —C(4)	116.5052
		N(7) —C(3) —C(2)	123.5420
		C(4) —C(3) —C(2)	119.9522
		C(3) —C(2) —C(1)	119.6851
		C(6) —C(1) —C(2)	120.0495

proportionally increased with concentration. The tested compounds before and after γ-irradiation are found to have remarkable biological activities. The results indicated that Ru^{3+} complexes exhibited a potent antibacterial activity. The antibacterial activities of the experienced ligand and complexes against *E. coli* were found to follow the order: Ru^{3+} > Pd^{2+} > Ag$^+$ > Zn^{2+} > VO^{2+} > Hg^{2+} > Mn^{2+} > H$_2$L for 1 μg before γ-irradiation. While, antibacterial activities of 5 μg/ml, 7 μg/ml and 10 μg/ml followed the order Ru^{3+} > Hg^{2+} > Pd^{2+} > H$_2$L > VO^{2+} > Mn^{2+} > Zn^{2+} > Ag$^+$ before γ-irradiation. Alternatively, antibacterial activity was evidenced when using the compound and metal complexes with *S. pyoge-*

Table S2 Selected bond lengths (Å) and angles (°) of Mn complex (B₂).

B₂ Complex			
Bond length		Bond angles	
O(64) —O(65)	1.5366	O(65) —O(64) —S(61)	137.6738
S(61) —O(64)	2.2716	O(64) —S(61) —O(63)	120.6658
S(61) —O(63)	1.4437	O(64) —S(61) —O(62)	119.0202
S(61) —O(62)	1.4394	O(64) —S(61) —Mn(28)	127.9320
C(52) —C(53)	1.3848	O(63) —S(61) —O(62)	117.2055
C(51) —C(52)	1.3860	O(63) —S(61) —Mn(28)	80.4077
C(50) —C(51)	1.3916	O(62) —S(61) —Mn(28)	78.3179
C(49) —C(50)	1.4064	C(52) —C(53) —C(48)	127.6463
C(48) —C(53)	1.3898	C(53) —C(52) —C(51)	116.4294
C(48) —C(49)	1.4281	C(52) —C(51) —C(50)	120.6844
N(47) —C(48)	1.4617	C(51) —C(50) —C(49)	117.6728
C(45) —N(47)	1.5120	C(50) —C(49) —C(48)	125.1593
C(43) —C(45)	1.5202	C(53) —C(48) —C(49)	110.2287
C(43) —O(44)	1.2056	C(53) —C(48) —N(47)	116.1241
N(42) —C(43)	1.2552	C(49) —C(48) —N(47)	133.4698
N(39) —N(42)	1.3246	C(48) —N(47) —C(45)	133.7278
C(38) —S(41)	1.5706	N(47) —C(45) —C(43)	123.0580
C(38) —N(39)	1.4823	C(43) —O(44) —Mn(28)	112.8550
N(37) —C(38)	1.3237	C(45) —C(43) —O(44)	122.2653
C(34) —Cl(36)	1.7138	C(45) —C(43) —N(42)	146.3721
C(34) —C(35)	1.4048	O(44) —C(43) —N(42)	91.0951
C(33) —C(34)	1.3923	C(43) —N(42) —N(39)	151.7469
C(32) —C(33)	1.3740	N(42) —N(39) —C(38)	120.1909
C(31) —N(37)	1.3869	N(42) —N(39) —Mn(28)	72.1193
C(31) —C(32)	1.4047	C(38) —N(39) —Mn(28)	119.2748
C(30) —C(35)	1.4056	S(41) —C(38) —N(39)	111.8708
C(30) —C(31)	1.4097	S(41) —C(38) —N(37)	113.0722
Mn(28) —S(61)	2.4755	N(39) —C(38) —N(37)	135.0570
Mn(28) —O(58)	1.9655	C(38) —N(37) —C(31)	125.3202
Mn(28) —O(44)	2.0268	C(34) —C(35) —C(30)	116.7059
Mn(28) —N(39)	2.1198	Cl(36) —C(34) —C(35)	126.5660
C(23) —C(24)	1.3969	Cl(36) —C(34) —C(33)	114.8739
C(22) —C(23)	1.3900	C(35) —C(34) —C(33)	117.9840
C(21) —C(22)	1.3908	C(34) —C(33) —C(32)	105.7759
C(20) —C(21)	1.4020	C(33) —C(32) —C(31)	111.3388
C(19) —C(24)	1.3970	N(37) —C(31) —C(32)	119.0564
C(19) —C(20)	1.4121	N(37) —C(31) —C(30)	132.1366
N(18) —C(19)	1.4445	C(32) —C(31) —C(30)	108.3607
C(16) —N(18)	1.5109	C(35) —C(30) —C(31)	118.3432
O(15) —Mn(28)	1.9317	S(61) —Mn(28) —O(58)	80.9487
C(14) —C(16)	1.5081	S(61) —Mn(28) —O(44)	87.0828
C(14) —O(15)	1.2272	S(61) —Mn(28) —N(39)	95.1401
N(13) —C(14)	1.2675	S(61) —Mn(28) —O(15)	175.5241
N(10) —Mn(28)	2.0354	S(61) —Mn(28) —N(10)	102.6261
N(10) —N(13)	1.3621	O(58) —Mn(28) —O(44)	167.1509
C(9) —S(12)	1.5935	O(58) —Mn(28) —N(39)	91.9307
C(9) —N(10)	1.4569	O(58) —Mn(28) —O(15)	94.8468
N(8) —C(9)	1.3153	O(58) —Mn(28) —N(10)	105.4010
C(5) —Cl(7)	1.7615	O(44) —Mn(28) —N(39)	84.4618
C(5) —C(6)	1.6584	O(44) —Mn(28) —O(15)	96.9765
C(4) —C(5)	1.6045	O(44) —Mn(28) —N(10)	81.6900
C(3) —C(4)	1.6056	N(39) —Mn(28) —O(15)	83.4170
C(2) —N(8)	1.4023	N(39) —Mn(28) —N(10)	156.7942
C(2) —C(3)	1.6962	O(15) —Mn(28) —N(10)	79.9041
C(1) —C(2)	1.7391	C(23) —C(24) —C(19)	123.2279
		C(24) —C(23) —C(22)	120.5888
		C(23) —C(22) —C(21)	117.5739
		C(22) —C(21) —C(20)	118.5725
		C(21) —C(20) —C(19)	125.0747
		C(24) —C(19) —C(20)	111.7476
		C(24) —C(19) —N(18)	123.1367

Table S2 (*continued*)

B₂ Complex

Bond length	Bond angles	
	C(20)—C(19)—N(18)	124.5001
	C(19)—N(18)—C(16)	133.8050
	N(18)—C(16)—C(14)	112.2615
	Mn(28)—O(15)—C(14)	115.6732
	C(16)—C(14)—O(15)	122.6012
	C(16)—C(14)—N(13)	119.4036
	O(15)—C(14)—N(13)	117.0367
	C(14)—N(13)—N(10)	121.1213
	Mn(28)—N(10)—N(13)	104.3028
	Mn(28)—N(10)—C(9)	119.4383
	N(13)—N(10)—C(9)	111.0143
	S(12)—C(9)—N(10)	124.2623
	S(12)—C(9)—N(8)	119.0867
	N(10)—C(9)—N(8)	114.4181
	C(9)—N(8)—C(2)	130.0752
	C(5)—C(6)—C(1)	120.1778
	Cl(7)—C(5)—C(6)	119.3424
	Cl(7)—C(5)—C(4)	19.1887
	C(6)—C(5)—C(4)	120.4980
	C(5)—C(4)—C(3)	122.7399
	C(4)—C(3)—C(2)	119.7557
	N(8)—C(2)—C(3)	112.9010
	N(8)—C(2)—C(1)	127.3640
	C(3)—C(2)—C(1)	116.9999
	C(6)—C(1)—C(2)	119.5663

Table S3 Selected bond lengths (Å) and angels (°) of Mn complex (B₂).

B₅ Complex

Bond length		Bond angles	
Pd(28)—Cl(30)	2.2962	Cl(30)—Pd(28)—Cl(29)	84.8166
Pd(28)—Cl(29)	2.3366	Cl(30)—Pd(28)—O(15)	82.0702
C(23)—C(24)	1.4250	Cl(30)—Pd(28)—N(10)	91.4175
C(22)—C(23)	1.3798	Cl(29)—Pd(28)—O(15)	84.4103
C(21)—C(22)	1.3954	Cl(29)—Pd(28)—N(10)	175.9945
C(20)—C(21)	1.3814	O(15)—Pd(28)—N(10)	93.7334
C(19)—C(24)	1.4275	C(23)—C(24)—C(19)	115.6252
C(19)—C(20)	1.4103	C(24)—C(23)—C(22)	122.9319
N(18)—C(19)	1.4370	C(23)—C(22)—C(21)	119.8203
C(16)—N(18)	1.4904	C(22)—C(21)—C(20)	119.5132
O(15)—Pd(28)	2.0015	C(21)—C(20)—C(19)	121.2321
C(14)—C(16)	1.4947	C(24)—C(19)—C(20)	120.3784
C(14)—O(15)	1.3351	C(24)—C(19)—N(18)	124.2776
N(13)—C(14)	1.4522	C(20)—C(19)—N(18)	115.0896
N(10)—Pd(28)	1.9935	C(19)—N(18)—C(16)	121.9717
N(10)—N(13)	1.5418	N(18)—C(16)—C(14)	108.1478
C(9)—S(12)	1.6337	Pd(28)—O(15)—C(14)	91.1223
C(9)—N(10)	1.4791	C(16)—C(14)—O(15)	121.7885
N(8)—C(9)	1.4651	C(16)—C(14)—N(13)	127.2815
C(5)—Cl(7)	1.6848	O(15)—C(14)—N(13)	110.5833
C(5)—C(6)	1.3859	C(14)—N(13)—N(10)	103.9664
C(4)—C(5)	1.3964	Pd(28)—N(10)—N(13)	93.5552
C(3)—C(4)	1.3834	Pd(28)—N(10)—C(9)	122.5539
C(2)—N(8)	1.4446	N(13)—N(10)—C(9)	113.6598
C(2)—C(3)	1.4047	S(12)—C(9)—N(10)	123.8522
C(1)—C(6)	1.4158	S(12)—C(9)—N(8)	124.2674
C(1)—C(2)	1.4263	N(10)—C(9)—N(8)	111.2228
		C(9)—N(8)—C(2)	115.5962

Table S3   (*continued*)

B$_5$ Complex	
Bond length	**Bond angles**
	C(5) —C(6) —C(1) 121.0817
	Cl(7) —C(5) —C(6) 119.3014
	Cl(7) —C(5) —C(4) 119.5419
	C(6) —C(5) —C(4) 121.1561
	C(5) —C(4) —C(3) 119.1813
	C(4) —C(3) —C(2) 120.7993
	N(8) —C(2) —C(3) 119.2049
	N(8) —C(2) —C(1) 120.0554
	C(3) —C(2) —C(1) 120.5987
	C(6) —C(1) —C(2) 117.1317

Table S4   Selected bond lengths (Å) and angels (°) of Hg complex (B$_7$).

B$_7$ Complex			
Bond length		**Bond angles**	
Hg(28) —Cl(30)	2.2680	Cl(30) —Hg(28) —Cl(29)	150.5859
Hg(28) —Cl(29)	2.3082	Cl(30) —Hg(28) —O(15)	99.7028
C(23) —C(24)	1.3907	Cl(30) —Hg(28) —N(10)	123.1647
C(22) —C(23)	1.3909	Cl(29) —Hg(28) —O(15)	88.4495
C(21) —C(22)	1.3909	Cl(29) —Hg(28) —N(10)	85.8140
C(20) —C(21)	1.3893	O(15) —Hg(28) —N(10)	81.9673
C(19) —C(24)	1.3996	C(23) —C(24) —C(19)	119.3978
C(19) —C(20)	1.4007	C(24) —C(23) —C(22)	120.5707
N(18) —C(19)	1.4509	C(23) —C(22) —C(21)	119.9143
C(16) —N(18)	1.4850	C(22) —C(21) —C(20)	120.2707
O(15) —Hg(28)	2.0983	C(21) —C(20) —C(19)	119.7403
C(14) —C(16)	1.5229	C(24) —C(19) —C(20)	120.1041
C(14) —O(15)	1.2376	C(24) —C(19) —N(18)	120.5004
N(13) —C(14)	1.4250	C(20) —C(19) —N(18)	119.2458
N(10) —Hg(28)	2.1511	C(19) —N(18) —C(16)	115.8452
N(10) —N(13)	1.4696	N(18) —C(16) —C(14)	110.3420
C(9) —S(12)	1.6505	Hg(28) —O(15) —C(14)	112.2937
C(9) —N(10)	1.4818	C(16) —C(14) —O(15)	121.2779
N(8) —C(9)	1.3850	C(16) —C(14) —N(13)	118.7978
C(5) —Cl(7)	1.6757	O(15) —C(14) —N(13)	119.6768
C(5) —C(6)	1.3952	C(14) —N(13) —N(10)	117.8180
C(4) —C(5)	1.3996	Hg(28) —N(10) —N(13)	103.6116
C(3) —C(4)	1.3866	Hg(28) —N(10) —C(9)	107.4776
C(2) —N(8)	1.4395	N(13) —N(10) —C(9)	112.7155
C(2) —C(3)	1.4178	S(12) —C(9) —N(10)	123.6712
C(1) —C(6)	1.3960	S(12) —C(9) —N(8)	121.1920
C(1) —C(2)	1.4098	N(10) —C(9) —N(8)	115.0862
		C(9) —N(8) —C(2)	131.8349
		C(5) —C(6) —C(1)	120.3232
		Cl(7) —C(5) —C(6)	119.8494
		Cl(7) —C(5) —C(4)	119.7000
		C(6) —C(5) —C(4)	120.4505
		C(5) —C(4) —C(3)	119.8282
		C(4) —C(3) —C(2)	120.3443
		N(8) —C(2) —C(3)	115.7849
		N(8) —C(2) —C(1)	124.5294
		C(3) —C(2) —C(1)	119.3455
		C(6) —C(1) —C(2)	119.7007

nes followed the order: Ag$^+$ > H$_2$L > Hg^{2+} > Zn^{2+} > Pd^{2+} > Ru^{3+} > Mn^{2+} > VO^{2+} with 1 µg/ml concentration (Hanaa et al., 2016). While, antibacterial activities of 5 µg/ml, 7 µg/ml and 10 µg/ml concentrations of compounds was in the following order: Hg(II) > Ru^{3+} > Ag$^+$ > H$_2$L > Mn^{2+} > Zn^{2+} > Pd^{2+} > VO^{2+} (Mehmet et al., 2010). The complexes

Table 4 The selected bond length (Å) of the ligand, Mn(II), Pd(II) and Hg(II) complexes.

Compound	Bond length						
	N7—C8 (L)	C8—N9 (L)	N9—N10 (L)	N10—C11 (L)	C11—O21 (L)	C11—C12 (L)	C12—N13 (L)
Ligand	1.38	1.45	1.43	1.45	1.22	1.52	1.48
	N8—C9	C9—N10	N10—N13	N13—C14	C14—O15	C14—C16	C16—N18
Mn(II)	1.32	1.46	1.36	1.27	1.23	1.51	1.51
	1.32	1.48	1.32	1.26	1.21	1.52	1.51
Pd(II)	1.47	1.48	1.54	1.45	1.34	1.49	1.49
Hg(II)	1.39	1.48	1.47	1.43	1.24	1.52	1.49

Table 5 The energetic properties of the ligand(B), Mn(II), Pd(II) and Hg(II) complexes.

The assignment of the theoretical parameters	Compound			
	Ligand	Mn	Pd	Hg
Total energy, Kcal/mol	−3567.1399	−8513.814	−4220.632	−3989.931
Binding energy, Kcal/mol	−3713.8618	−8551.775	−4235.8677	−4006.8366
Potential energy, Kcal/mol	−79422.940	−207356.48	−118384.797	−94919.801
Isolated Atomic Energy, Kcal/mol	−75709.078	−198804.706	−114148.929	−90912.965
Electronic Energy, Kcal/mol	−548786.102	−2509439.00	−877684.483	−696512.888
Core-Core Interaction, Kcal/mol	469363.162	2302082.52	759299.686	601593.087
Heat of Formation	237.9671	−59.9166	−136.058	17.6623
Dipole moment (Debye)	2.878	6.234	11.426	5.841
HOMO (eV)	−8.414	−7.287	−7.419	−9.465
LUMO (eV)	−1.592	−1.652	−1.894	−2.291

Table 6 Antibacterial activity for the ligand and its metal complexes before and after irradiation against *S. pyogenes*.

Compound	Inhibition %			
	S. pyogenes			
	1 µg/ml	5 µg/ml	7 µg/ml	10 µg/ml
H_2L	82.50	94.23	96	98
H_2L *	82.88	96.00	97	99
$VO(HL)_2$	58	65	70	75
$VO(HL)_2$*	70.19	94.23	97	99
$Mn(H_2L)_2SO_4·2H_2O$	64.23	82.88	85	90
$Mn(H_2L)_2SO_4·2H_2O$*	90.38	94.8	96.5	98
$Zn(H_2L)_2SO_4$	66.33	79.66	80	85
$Zn(H_2L)_2SO_4$*	89.66	94.5	92	97
$Ru(HL)_3$	64.5	96.16	98	99.3
$Ru(HL)_{3*}$	89.5	98.33	99	99.6
$Pd(H_2L)Cl_2·½ETOH$	65.57	67.11	73	79
$Pd(H_2L)Cl_2·½ETOH$*	90	95.4	93	97
$Ag(H_2L)(HL)H_2O·½ETOH$	94.23	96	98	99
$Ag(H_2L)(HL)H_2O·½ETOH$*	74.42	95.38	97	99.6
$Hg(H_2L)Cl_2·½H_2O$	80.19	99.23	99.5	99.8
$Hg(H_2L)Cl_2·½H_2O$*	91.53	95.19	96	98

Where * after gamma irradiation (6Mega Rad).

formation could make the penetration across the cell membrane of *E. coli* easier and can be elucidated by Tweedy's chelation theory (Tweedy, 1964). Chelation could improve the lipophilic character of the central metal atom which in rotate, which improved its penetration through the lipoid layer of the membrane thus causing the metal complex to cross the bacterial membrane more successfully thus increasing the activity of the complexes. In addition, many other reasons for instance solubility, dipole moment, conductivity influenced by metal ion may be probable causes for amazing antibacterial activities of these complexes (Chohan et al., 2006). Exposure to γ-irradiation remarkably enhanced the antibacterial activity for both the ligand and its complexes when it was used in case of *E. coli*. The activity also increased after irradiation in case of *S. pyogenes*. This may be attributed to the different nature of the cell wall for both microbes which may be correlated with

Table 7 Antibacterial activity for the ligand and its metal complexes before and after irradiation *E. Coli.*

Compound	Inhibition %			
			E. coli	
	1 µg/ml	5 µg/ml	7 µg/ml	10 µg/ml
H_2L	59.66	91.66	94	96
H_2L*	76.16	97.11	98	99.2
$VO(HL)_2$	82.16	87	92	94
$VO(HL)_2$*	92.6	96.83	97.8	98.7
$Mn(H_2L)_2SO_4 \cdot 2H_2O$	77.83	86.50	90.7	93.5
$Mn(H_2L)_2SO_4 \cdot 2H_2O$*	78.16	95.16	97	99
$Zn(H_2L)_2SO_4$	82.8	85.8	90	94
$Zn(H_2L)_2SO_4$*	86.4	92.4	95.5	99
$Ru(HL)_3$	91	95.4	95	99
$Ru(HL)_{3*}$	93.6	96.8	96	99.2
$Pd(H_2L)Cl_2 \cdot \frac{1}{2}ETOH$	88	92.6	94	96
$Pd(H_2L)Cl_2 \cdot \frac{1}{2}ETOH$*	93.83	94.83	96	98
$Ag(H_2L)(HL)H_2O \cdot \frac{1}{2}ETOH$	79.91	83	86	92
$Ag(H_2L)(HL)H_2O \cdot \frac{1}{2}ETOH$*	85.66	97	90	99
$Hg(H_2L)Cl_2 \cdot \frac{1}{2}H_2O$	82	93.4	95	97
$Hg(H_2L)Cl_2 \cdot \frac{1}{2}H_2O$*	93.2	100	100	100

Where * after gamma irradiation (6Mega Rad).
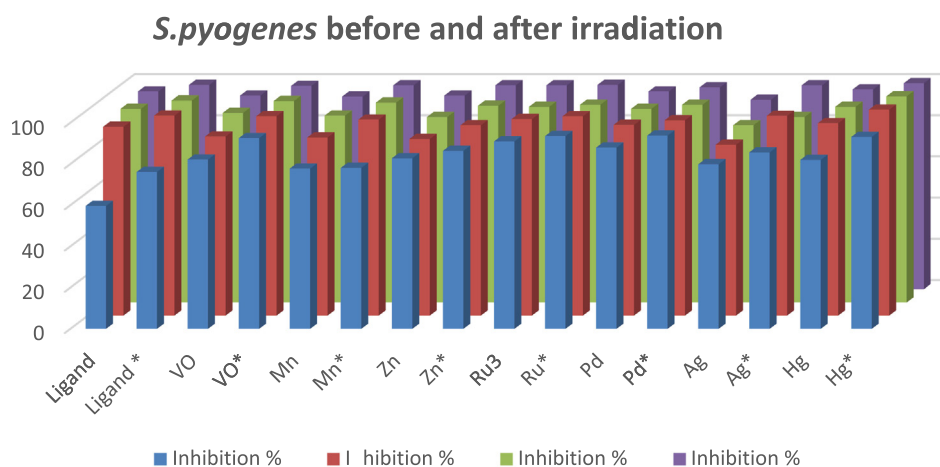
Fig. 9 Antibacterial activity for the ligand and its metal complexes before and after irradiation against *S. pyogenes.*
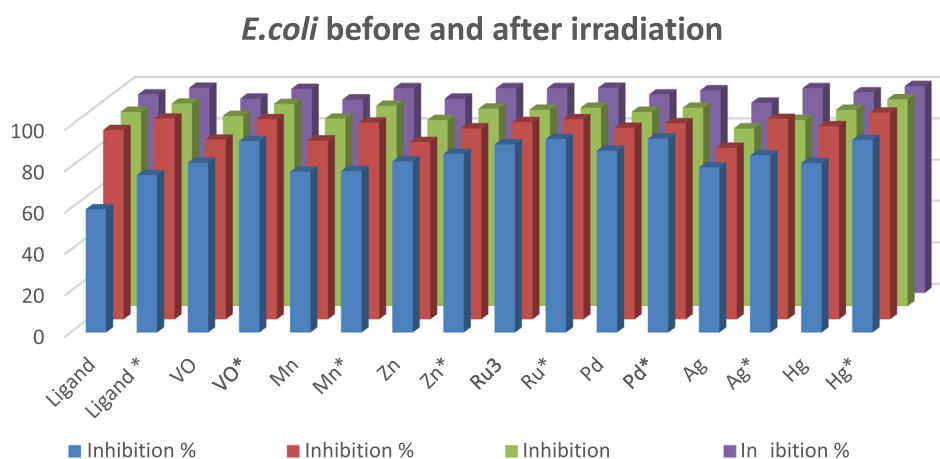
Fig. 10 Antibacterial activity for the ligand and its metal complexes before and after irradiation against *E. coli.*

the above factors (Mehmet et al., 2010). Additionally, exposure to γ-irradiation increased the antibacterial activity of both the free a cyclic ligand and their complexes when used with both concentrations (1 μg/ml, 5 μg/ml, 7 μg/ml and 10 μg/ml) in case of the Gram positive *S. pyogenes* bacterium. It was also observed that some moieties for instance N(2)H linkage introduced into such compounds exhibits widespread biological that may be accountable for raise in hydrophobic nature and lipo-solubility of the molecules in crossing the cell membrane of the bacteria and augment biological consumption ratio and activity of complexes activity (Har et al., 2016; Huang et al., 2018, 2019; Zhenzhen et al., 2017). It is concluded that these compounds have antibacterial activities and can be used in the future as therapeutic drugs for bacterial diseases.

4. Conclusions

In summary, the effect of high energetic gamma ray on VO^{2+}, Mn^{2+}, Zn^{2+}, Ru^{3+}, Pd^{2+}, Ag^+ and Hg^{2+} of thiosemicarbazone ligand have been studied by different analytical and spectroscopic methods. The result confirmed the following:

- The ligand behaves as mono basic tetradentate in complex B_1 or neutral bi, tetradentate in complexes B_5, B_7 and B_2, B_3, B_6, respectively.
- ^{1}H NMR and IR exhibit higher intensity of the bands by using radiation
- γ-ray improve the thermal stability of the compounds by using TGA.
- X-ray diffraction pattern after irradiation show that the amorphous nature of the complexes changed to highly crystalline materials with high intensity and sharp line of diffraction.
- γ-ray confirmed some better determined in structures with an remarkably higher absorbance and no change in the geometry of metal complexes
- The suggested structures of complexes were geometrically adjusted and their structural limits were calculated. The computational calculations confirmed that B_5 and B_7 complexes have square planer geometry but Mn^{2+} complex has octahedral geometry, this is also in a good contract with the trial results.
- In vitro antibacterial activity showed that these chelates exhibited amazing antibacterial activity which increases after irradiation for some compound.

Declaration of Competing interest

The authors declare that they have no conflict of interest.

References

Adly, O.M., 2011. Synthesis, molecular modeling, thermal and spectral studies of metal complexes of hydrazone derived from 5-acetyl-4-hydroxy-2H-1,3-thiazine-2,6(3H)-dione and thiosemicarbazide. Spectrochim. Acta A 79, 1295–1303. https://doi.org/10.1016/j.saa.2011.04.058.

Ahmed, H.O., 2006. Synthesis and characterization of Cobalt(II) and Nickel(II) complexes of some Schiff bases derived from 3-hydrazino-6-methyl[1,2,4] triazin-5(4H)one. Trans. Met. Chem. 31, 35–41. https://doi.org/10.1007/s11243-005-6265-7.

Aliakbar, D.K., Ensieh, S., Nourollah, F., Monika, K., Michal, D., Raouf, M., 2017. Silver(I) thiosemicarbazone complex [Ag(catsc)(PPh₃)₂]NO₃: synthesis, characterization, crystal structure, and antibacterial study. C. R. Chim. 20, 534–539. https://doi.org/10.1016/j.crci.2016.09.001.

Bassett, J., Denney, R.C., Jeffery, G.H., Mendham, J., 1978. Vogel's Textbook of Quantitative Inorganic Analysis Including Elementary Instrumental Analysis. Longman Group, London, p. 316.

Benson, R.S., 2002. Nucl. Instrum. Meth. Phys. Res. Sect. B 191, 752. https://doi.org/10.1016/j.saa.2014.11.015.

Chandra, S., Kumar, U., 2005. Spectral and magnetic studies on manganese(II), cobalt(II) and nickel(II) complexes with Schiff bases. Spectrochim. Acta A 61, 219–224. https://doi.org/10.1016/j.saa.2004.03.036.

Chohan, Z.H., Shaikh, A.U., Rauf, A., Supuran, C.T., 2006. Antibacterial, antifungal and cytotoxic properties of novel N-substituted sulfonamides from 4-hydroxycoumarin. J. Enz. Inhib. Med. Chem. 21, 741–748. https://doi.org/10.1080/14756360600810340.

Elena, L.T., Ma, A.M., Jesus, R., Ma, T.S., Enrique, C., Jose, M.M., Isabel, S., 2001. Synthesis and characterisation of zinc, cadmium and mercury complexes of benzilbisthiosemicarbazone. Structure of cadmium derivative. Inorg. Chim. Acta 323, 130–138. https://doi.org/10.1016/S0020-1693(01), 00607-7.

Gavhane, V.S., Anjali, S.R., Suresh, T.G., 2015. X-ray diffraction study and biological analysis of transition metal complexes of N-4-disubstituted thiosemicarbazone. Res. J. Chem. Sci. 5, 33–37.

Gustavo, S.C., Pedro, P.C., Camilla, A., André, L.B., Wilton, R.L., Alexandre, C., 2012. Silver(I) and gold(I) complexes with penicillamine: synthesis, spectroscopic characterization and biological studies. Polyhedron 34, 210–214. https://doi.org/10.1016/j.poly.2012.01.002.

Geary, W.J., 1971. The use of conductivity measurements in organic solvents for the characterisation of coordination compounds. Coord. Chem. Rev. 7, 81–122. https://doi.org/10.1016/S0010-8545(00), 80009-0.

Geeta, B., Shravankumar, K., Reddy, P.M., Ravikrishna, E., Sarangapani, M., Reddy, K.K., Ravinder, V., 2010. Binuclear cobalt(II), nickel(II), copper(II) and palladium(II) complexes of a new Schiff-base as ligand: synthesis, structural characterization, and antibacterial activity. Spectrochim. Acta A 77, 911–915. https://doi.org/10.1016/j.saa.2010.08.004.

Hanaa, A., Ocala, A., 2015. New 15-membered tetraaza (N4) macrocyclic ligand and its transition metal complexes: spectral, magnetic, thermal and anticancer activity. Spectrochim. Acta Part A 138, 553–562.

Hanaa, A., Mogda, A., Abla, A.H., 2016. Macrocyclic [N₅] transition metal complexes: synthesis, characterization and biological activities. J Inclu. Phenom. Macrocyclic Chem. 86, 153–166. https://doi.org/10.1007/s10847-016-0649-5.

Har, L.S., Singh, J.B., Sunta, B., 2016. Synthesis, spectral, DFT, and antimicrobial studies of tin(II) and lead(II) complexes with semicarbazone and thiosemicarbazones derived from (2-hydroxyphenyl)(pyrrolidin-1-yl)methanone. J. Coord. Chem. 69, 343–353. https://doi.org/10.1080/00958972.2015.1115485.

Huang, Z., Zeng, Z., Chen, A., Zeng, G., Xiao, R., Xu, P., He, K., Song, Z., Hu, L., Peng, M., Huang, T., Chen, G., 2018. Differential behaviors of silver nanoparticles and silver ions towards cysteine: Bioremediation and toxicity to Phanerochaete chrysosporium. Chemosphere 203, 199–208. https://doi.org/10.1016/j.chemosphere.2018.03.144.

Huang, Z., He, K., Song, Z., Zeng, G., Chen, A., Yuan, L., Li, H., Chen, G., 2019. Alleviation of heavy metal and silver nanoparticle toxicity and enhancement of their removal by hydrogen sulfide in Phanerochaete chrysosporium. Chemosphere 224, 554–561. https://doi.org/10.1016/j.chemosphere.2019.02.190.

HyperChem,Release 8.03 for Windows, Molecular Modeling System, Hypercube Inc. 2007.

Jeragh, B., El-Asmy, A.A., 2014. Coordination of Fe(III), Co(II), Ni(II), Cu(II), Zn(II), Cd(II), Hg(II), Pd(II) and Pt(II) with 2,5-hexanedione bis(thiosemicarbazone), HBTS: crystal structure of

cis-[Pd(HBTS)]Cl$_2$ and 1-(2,5-dimethyl-1H-pyrrol-yl)-thiourea. Spectrochim. Acta A 130, 546–552. https://doi.org/10.1016/j.saa.2014.04.013.

Jayashri, T.A., Krishnan, G., Rani, N.R., 2014. Effect of gamma-irradiation on thermal decomposition kinetics, X-ray diffraction pattern and spectral properties of tris(1,2- diaminoethane) nickel (II) sulphate. Radiat. Effects Defects Solids 169, 1019–1030. https://doi.org/10.1080/10420150.2014.980257.

Krishnan, S., Laly, K., Prathapachandra, M.R., 2010. Synthesis and spectral investigations of Mn(II) complexes of pentadentate bis (thiosemicarbazones). Spectrochim. Acta 75, 585–588. https://doi.org/10.1016/j.saa.2009.11.022.

Maany, M.H., Ola, E., Ahmed, A.E., 2006. Enhancement of the catalytic activity of [Cu$_2$(TS)(OH)$_2$(OAc)] using superconductor cuprate sample. Trans. Met. Chem. 31, 714–719. https://doi.org/10.1007/s11243-006-0054-9.

Morsy, M.A., Tahani, I.K., Samar, A.A., 2011. Spectrochemical study and effect of high energatic gamma ray on copper (II) complexes. J. Solid State Sci. 13, 2080–2085. https://doi.org/10.1016/j.solidstatesciences.2011.07.015.

Murali, P.K., Hussain, R., 2009. Synthesis, single crystal structure and DNA cleavage studies on first 4-N-ethyl substituted three coordinate copper(I) complex of thiosemicarbazone. Inorg. Chim. Acta 362, 4185–4190. https://doi.org/10.1016/j.ica.2009.06.022.

Mehmet, S., Metin, C., Ismet, B., 2010. Synthesis, spectroscopic and biological studies on the new symmetric Schiff base derived from 2,6-diformyl-4-methylphenol with N-aminopyrimidine. Eur. J. Med. Chem. 45, 1935–1940. https://doi.org/10.1016/j.ejmech.2010.01.035.

Mohamed, G., Hoda, E., Faten, A., Shaimaa, F., 2015. Synthesis, spectral and theoretical studies of Ni(II), Pd(II) and Pt(II) complexes of 5-mercapto-1,2,4-triazole-3-imine-2'- hydroxynaphthaline. Spectrochim Acta A 137, 919–929. https://doi.org/10.1016/j.saa.2014.09.015.

Nabil, S.Y., Hegab, K.H., 2005. Synthesis and characterization of some transition metal complexes of thiosemicarbazones derived from 2-acetylpyrrole and 2-acetylfuran. Synth. React. Inorg. Metal-Org. Nano-Met. Chem. 35, 391–399. https://doi.org/10.1081/SIM -200059215.

Nadia, D., Yang, F., Bohari, M.Y., Nazlina, I., 2017. Synthesis, structural, chemical properties, and anti-bacterial screening of Sm (III) thiosemicarbazone complexes. Malaysian J. Anal. Sci. 21, 560–570. https://doi.org/10.17576/mjas-2017-2103-06.

Piyali, P., Ray, J.B., Samaresh, B., 2015. Palladium complexes of 2-formylpyridine thiosemicarbazone and two related ligands: synthesis, structure and spectral and catalytic properties. Inorg. Chim. Acta 425, 67–75. https://doi.org/10.1016/j.ica.2014.10.010.

Raja, N., Ramesh, R., 2010. Mononuclear ruthenium(III) complexes containing chelating thiosemicarbazones: synthesis, characterization and catalytic property. Spectrochim. Acta A 75, 713–718. https://doi.org/10.1016/j.saa.2009.11.044.

Samar, A.A., Ayman, S., 2017. Synthesis, characterization of new copper complexes of thiosemicarbazone derivatives and their biological activities. Int. J. Res. Chem. Environ. 7, 38–46.

Samar, A.A., 2017. Spectrochemical study the effect of high energetic ionization radiation on Ru(III), Pd(II) and Hg(II) complexes. J. Rad. Res. App. Sci. 10, 89–96. https://doi.org/10.1016/j.jrras.2016.12.001.

Seena, E.B., Kurup, M.P., 2007. Synthesis, spectral and structural studies of zinc(II) complexes of salicylaldehyde N4-phenylthiosemi-carbazone. Spectrochim Acta A. 69, 726–732. https://doi.org/10.1016/j.saa.2007.05.025.

Singh, A., Bharty, M.K., Dani, R.K., Singh, S., Kushawaha, S.K., Singh, N.K., 2014. Manganese(II) and zinc(II) complexes of 4-phenyl(2-methoxybenzoyl)-3- thiosemicarbazide: synthesis, spectral, structural characterization, thermal behavior and DFT study. Polyhedron 73, 98–109. https://doi.org/10.1016/j.poly.2014.02.029.

Sanaa, M.E., El Sayed, I.E., Nassar, N., 2015. Transition metal complexes of neocryptolepine analogues. Part I: synthesis, spectroscopic characterization, and in vitro anticancer activity of copper(II) complexes. Spectrochim. Acta A 138, 942–953. https://doi.org/10.1016/j.saa.2014.03.114.

Seda, S., Baybars, K., Fatma, K., Sevgi, H.B., 2009. Theoretical and spectroscopic studies of 5-fluoro-isatin-3- (N-benzylthiosemicar-bazone) and its zinc(II) complex. J. Mol. Struct. 917, 63–70. https://doi.org/10.1016/j.molstruc.2008.06.033.

Tweedy, B.G., 1964. Plant extracts with metal ions as potential antimicrobial agents. Phytopathology 55, 910–914.

Uarikumaran, M.L., Appukuttan, A.S., 2012. Syntheses, spectral, surface morphological and gamma ray irradiation studies of some oxomolybdenum(V) and dioxomolybdenum(VI) complexes of an azo dye derived from 4-aminoantipyrine. J. Korean Chem. Soc. 56, 217–227. https://doi.org/10.5012/jkcs.2012.56.2.217.

Yousef, T.A., Rakha, T.H., Usama, E., Abu El Reash, G.M., 2012. Synthesis, spectroscopic characterization and thermal behavior of metal complexes formed with (Z)-2-oxo-2-(2-(2-oxoindolin-3-yli-dene)hydrazinyl)-N-phenylacetamide (H$_2$OI). J. Mol. Struct. 1007, 146–157. https://doi.org/10.1016/j.molstruc.2011.10.036.

Zhenzhen, H., Guiqiu, C., Guangming, Z., Zhi, G., Zhongxian, S., 2017. Toxicity mechanisms and synergies of silver nanoparticles in 2,4-dichlorophenol degradation by Phanerochaete chrysosporium. J. Hazard. Mater. 321, 37–46. https://doi.org/10.1016/j.jhazmat.2016.08.075.